Statistics of geodesics in large quadrangulations

J Bouttier and E Guitter

Service de Physique Théorique, CEA/DSM/SPhT, Unité de recherche associée au CNRS, CEA/Saclay, 91191 Gif sur Yvette Cedex, France

E-mail: jeremie.bouttier@cea.fr and emmanuel.guitter@cea.fr

Abstract
We study the statistical properties of geodesics, i.e. paths of minimal length, in large random planar quadrangulations. We extend Schaeffer's well-labeled tree bijection to the case of quadrangulations with a marked geodesic, leading to the notion of 'spine trees', amenable to a direct enumeration. We obtain the generating functions for quadrangulations with a marked geodesic of fixed length, as well as with a set of 'confluent geodesics', i.e. a collection of non-intersecting minimal paths connecting two given points. In the limit of quadrangulations with a large area n, we find in particular an average number 3×2^i of geodesics between two fixed points at distance $i \gg 1$ from each other. We show that, for generic endpoints, two confluent geodesics remain close to each other and have an extensive number of contacts. This property fails for a few 'exceptional' endpoints which can be linked by truly distinct geodesics. Results are presented both in the case of finite length i and in the scaling limit $i \propto n^{1/4}$. In particular, we give the scaling distribution of the exceptional points.

PACS numbers: 02.10.Ox, 05.50.+q, 04.60.Nc, 04.60.−m

(Some figures in this article are in colour only in the electronic version)

1. Introduction

The study of random maps is a fundamental issue both in mathematics, where it raises many interesting combinatorial and probabilistic problems, and in physics, where maps serve as discretizations for fluctuating surfaces in various domains. Understanding the statistical properties of ensembles of random maps is relevant, in particular, in the context of two-dimensional quantum gravity [1] or for the description of fluid membrane statistics. So far, most results deal with global properties of random maps, with much effort made on the *enumeration* of families of maps. Various methods were developed in this context, such as Tutte's original approach through recursive decomposition [2] or the more technical framework of random matrix integrals [3, 4]. Correlations functions of various observables were obtained

for ensembles of maps with possibly extra statistical degrees of freedom, such as spins or particles, but mostly in a global way consisting on averaging over the positions of the points where these observables are measured (see [4]). Much less is known on more refined local properties of maps, such as the actual dependence of correlations on the distance between the points where the observables are measured [5, 6]. In this respect, a particularly promising approach relies on a recent *bijective* enumeration technique which consists in a coding of maps by decorated trees. This approach was initiated by Schaeffer who found a one-to-one mapping between, on the one hand, planar quadrangulations, i.e. maps with tetravalent faces only, and on the other hand so-called *well-labeled trees*, i.e. plane trees with suitably labeled vertices [7, 8]. His construction was then extended to various families of maps, such as maps with prescribed faces valences [9], Eulerian maps and even maps with particles or spins [10]. The main advantage of the approach is that it keeps track of the graph distance of vertices from a given arbitrary origin vertex, thus giving access to statistical properties of maps controlled by this distance. A first application concerned the so-called *two-point function*, i.e. the average number of pairs of vertices at a fixed distance from each other among quadrangulations of fixed area. In particular, for large maps, this two-point function was shown to converge to a universal scaling function characterizing the density of vertices at a fixed distance from an arbitrary origin in the continuous scaling limit of large maps [5, 11].

In this paper, we address the question of the statistics of *geodesics*, i.e. paths which join two given vertices in a random quadrangulation, and are of minimal length among all paths linking these vertices. Here again, we rely on an extension of Schaeffer's bijection using well-labeled trees to code for quadrangulations with a marked geodesic path. In this setting, we have access to the statistical properties of geodesics with a fixed given length, as well as of *confluent geodesics*, i.e. collections of non-intersecting minimal paths connecting the same two vertices. Many results can be explicited in the limit of large quadrangulations, i.e. when the area of the quadrangulation tends to infinity. Two different regimes may be studied according to whether the length of the geodesics remains finite or scales as the appropriate power of the diverging area. This latter scaling regime is particularly important to extract universal properties characterizing the *continuous limit of large quadrangulations*, a probabilistic object whose construction is still under investigation [12–14].

The paper is organized as follows: section 2 is devoted to the combinatorics of quadrangulations with marked geodesics. We first recall in section 2.1 Schaeffer's construction, which associates to each quadrangulation a well-labeled tree. We then show in section 2.2 how to extend this bijection to treat the case of quadrangulations with a marked geodesic path. This leads to the notion of *spine tree*, i.e. a well-labeled tree with a distinguished linear subtree (the spine) inherited from the marked path. Spine trees are shown to be in bijection with quadrangulations equipped with a boundary made of two geodesics. Under the condition that these two boundary geodesics have no intermediate contact, the configurations can be continuously transformed into the desired configurations of quadrangulations with a single marked geodesic path. In section 2.3, we derive explicit formulae for the generating function of quadrangulations bounded by two geodesic paths and for that of quadrangulations with a single marked geodesic of given length. The connection between the two generating functions is obtained via a simple transformation consisting in taking an irreducible part. We finally show in section 2.4 how to use our basic generating functions to enumerate quadrangulations with marked confluent geodesics. We distinguish two general cases: weakly avoiding confluent geodesics made of paths that can touch each other with no intersections or strongly avoiding confluent geodesics which have no contact vertices except for their common first and last vertices. Section 3 deals with the statistical properties of geodesics of *finite length i* in large quadrangulations, i.e. in an ensemble of quadrangulations

with fixed area n in the limit $n \to \infty$, keeping i finite. We first explain in section 3.1 how our enumerative results can be translated into averages in the ensemble of pointed quadrangulations of fixed area n (with inverse symmetry weights) or the ensemble of quadrangulations with two marked points at fixed distance. We then give in section 3.2 the generating function for the average number of geodesics of length i in pointed quadrangulations with area $n \to \infty$. In particular, for large i, we obtain an average number 3×2^i of geodesics linking two given vertices at distance i. The average number of confluent geodesics is computed in section 3.3 and some of their refined properties are discussed in section 3.4, such as the average number of contacts between two weakly avoiding geodesics and the average area which they enclose. We finally discuss the case of strongly avoiding geodesics and show that, at large n, only a set of size $\propto n^{1/4}$ of *exceptional* points can be reached from a given vertex by two such strongly avoiding geodesics. In section 4, we study a different scaling regime in which the size n of the quadrangulation and the length i of the geodesics tend simultaneously to infinity, keeping the ratio $r = i/n^{1/4}$ fixed. This scaling is customary in the context of large quadrangulations, and we recall in section 4.1 the formula for the universal density $\rho(r)$ of vertices at a rescaled distance r from a given origin. We show in section 4.2 that upon appropriate renormalizations the average number of geodesics of rescaled length r, or of k-tuples of confluent geodesics, is characterized by the same scaling function $\rho(r)$. On the other hand, we show that the density of exceptional points is described by a new scaling function that we compute in section 4.3. We finally discuss in section 4.4 the area enclosed by two geodesics and show that this area is proportional to the total area n only in the case of strongly avoiding geodesics. We discuss our results and conclude in section 5.

2. Geodesics in quadrangulations and labeled trees

2.1. Schaeffer's construction for planar quadrangulations

In order to study maps with marked geodesics, we shall recourse to the well-known correspondence between rooted planar quadrangulations and so-called well-labeled trees [15] in the form found by Schaeffer *et al* [7, 8]. The correspondence works as follows: starting from a rooted planar quadrangulation, i.e. a quadrangulation of the sphere with a distinguished oriented edge, we label each vertex by its graph distance from the *origin*, i.e. the vertex from which the root edge originates. Each vertex therefore receives a strictly positive integer label, except for the origin which receives the label 0. It is easily seen that the faces of the quadrangulation fall into two classes (see figure 1): simple faces where the cyclic sequence of labels around the face is of the form $i, i + 1, i + 2, i + 1$ for some $i \geqslant 0$ and confluent faces where it is of the form $i, i + 1, i, i + 1$.

For each simple face, we select the unique edge of type $i + 2 \to i + 1$ encountered clockwise around the face (see figure 1(a)). For each confluent face, we draw a new edge linking the two vertices labeled $i + 1$ (see figure 1(b)). The procedure thus associates an edge to each face of the original quadrangulation, and it can be shown that the graph made of these edges connects all the original vertices except the origin that remains isolated. Furthermore, it is planar, contains no loop and has one more vertex than the edge, hence it is a plane tree (see figure 2 for an example). By construction, the labels on the vertices are strictly positive integers and vary by at most one along any edge of the tree. This property characterizes so-called *well-labeled* trees. The root edge of the quadrangulation selects a corner of the tree at its endpoint (labeled 1), at which we plant the tree. It was shown that the construction above provides a bijection between rooted planar quadrangulations and well-labeled trees planted at a corner labeled 1.
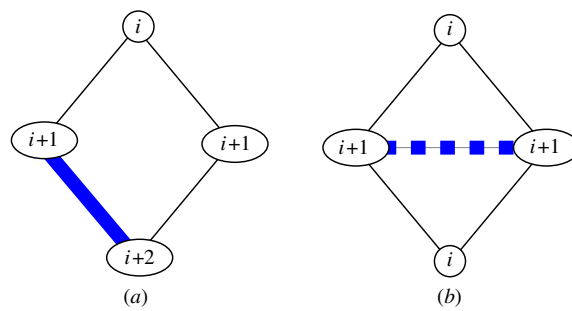
Figure 1. The two possible types of faces in a planar quadrangulation according to the distances of their incident vertices from a given origin: (*a*) simple faces and (*b*) confluent faces. To each face, we associate an edge of well-labeled tree (thick solid or dashed lines).
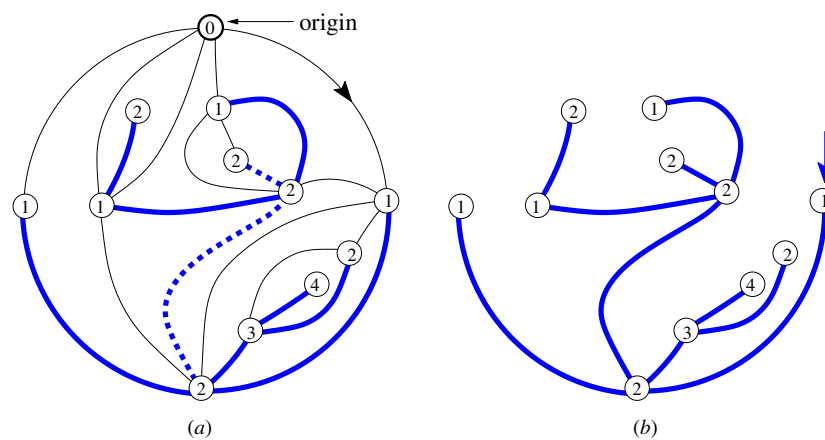

Figure 2. An example (*a*) of rooted quadrangulation (thick or thin solid lines) and the associated edges (thick solid or dashed lines) in Schaeffer's construction. These edges form a planted well-labeled tree (*b*).

The inverse construction can be realized as follows: starting from a well-labeled tree, we connect by an arch each corner with label $i > 1$ to its *successor*, that is the first corner labeled $i - 1$ encountered clockwise around the tree (see figure 3 for an example). Corners labeled 1 are then connected by arches to an extra vertex 0 outside the tree. The fact that labels vary by at most one along an edge ensures that the arches can be drawn with no intersection, resulting in a planar quadrangulation while the labels simply record the graph distance from the added vertex. The arch from the corner labeled 1 at which the tree was planted to the extra vertex, when oriented backwards, defines the root edge of the quadrangulation.

2.2. Extension to quadrangulations with a marked geodesic

We now turn to the study of quadrangulations with a marked geodesic, that is an oriented path connecting two vertices and having a minimal length among all paths connecting these vertices. The vertex from which the geodesic originates will be referred to as the origin vertex. Clearly, when moving along a geodesic, the distance from the origin of the successive vertices increases by one at each step. Note that picking a geodesic of length 1 simply amounts to
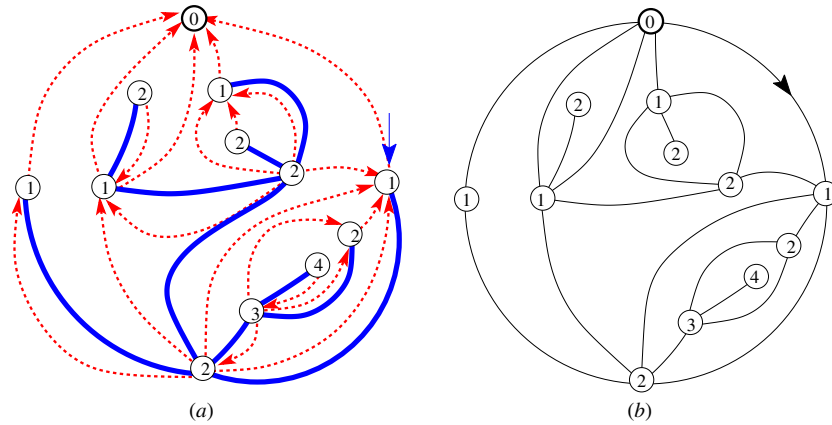
Figure 3. Construction of the quadrangulation associated with a given well-labeled tree. Corners are connected to their successors (*a*) by a set of non-crossing arches (dashed lines). These arches form the edges of the quadrangulation (*b*).
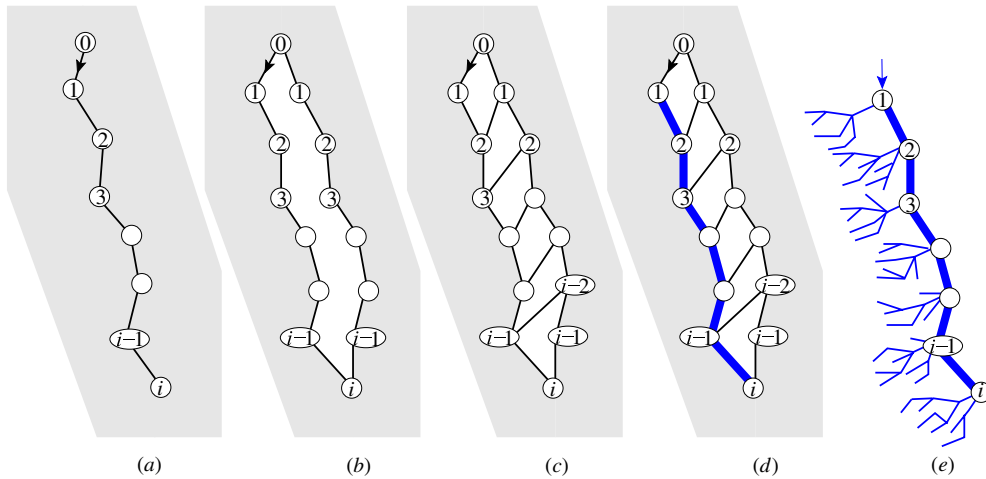

Figure 4. The extension of Schaeffer's construction to quadrangulations with a marked geodesic. In (*a*), we only display the marked geodesic, while the underlying quadrangulation is symbolized by the grey background. We first unzip the geodesic path (*b*) and fill the created hole by squares (*c*). Applying the rules of figure 1 for the added squares selects all the edges of the left copy of the geodesic but one (*d*), creating a spine (thick line). The original faces of the quadrangulation give rise to well-labeled subtrees attached only to the left side of this spine, resulting in a spine tree (*e*).

marking an oriented edge of the quadrangulation, in which case the object at hand is nothing but a rooted quadrangulation on which we may apply Schaeffer's construction. If the length i of the geodesic is larger than or equal to 2, it is then convenient to adapt this construction to ensure that all the edges of the geodesic path but the first one are selected and form a path of length $i - 1$ on the tree. To this end, we decide to first 'unzip' the geodesic so as to form a hole in the quadrangulation, bounded by two copies of the original geodesic (see figure 4), which we will refer to as the left and right copy upon viewing the hole with the origin at the top. We then fill up the hole with $i - 1$ new squares obtained by adding $i - 2$ parallel edges linking,

for each $k = 1, \ldots, i - 2$, the vertex of the right boundary at distance k from the origin to the vertex of the left boundary at distance $k + 1$. At this stage, it is important to note that both the unzipping process and the filling process *do not affect the distances* from the origin on the quadrangulation. In particular, both copies of the original geodesic are actual geodesic paths in the modified quadrangulation and their vertex labels indeed correspond to the distance from the origin. We finally root the modified quadrangulation by selecting the edge $0 \to 1$ of the left copy of the geodesic.

With this rooted quadrangulation at hand, we may now apply Schaeffer's construction and transform it into a well-labeled tree. By construction, all the added squares are simple faces of which we select the lowermost edge on the left boundary (see figure 4(*d*)). All the edges of the left boundary but the first one are therefore selected, thus forming a path of length $i - 1$ on the tree linking i vertices with increasing labels $1, 2, \ldots, i$. We shall call this path the spine of the tree. On the other hand, none of the added edges is selected and the rest of the tree is therefore made of i (possibly empty) subtrees attached only *to the left side* of the spine, when viewing it as hanging from its first vertex.

In view of this result, we are naturally led to define a *spine tree* as a particular type of well-labeled tree, made of a spine of length $i - 1$ joining i vertices with increasing labels $1, 2, \ldots, i$ and of i well-labeled subtrees attached to the left side of this spine. The tree is planted at the first vertex of the spine and can be viewed as hanging from that vertex.

With this definition, we see that applying Schaeffer's construction to our modified quadrangulation results in a spine tree. As we shall see below, not all spine trees however are obtained that way. This can be understood by first applying the inverse construction recalled in section 2.1 to a spine tree obtained as above from a quadrangulation with a marked geodesic and following how the two copies of the geodesic path are reconstructed. For each vertex along the spine with label $\geqslant 2$, the associated corner lying just on the left of the incident spine edge pointing toward the root gives rise to an arch linking that corner to the preceding vertex on the spine (see figure 5). This set of arches, together with the arch linking the root corner to the extra origin vertex labeled 0, forms the left copy of the geodesic path on the modified quadrangulation. On the other hand, consider now the vertex labeled i at the end of the spine and its chain of successors (i.e. its successor, the successor of its successor, etc): this chain forms the right copy of the geodesic. Furthermore, one easily sees that, for $j \geqslant 1$, the corner labeled $j + 1$ lying on the right of the spine will be connected by an arch winding around the tree to the vertex labeled j of the chain. Completing the inverse construction, the resulting object is the desired quadrangulation where the two copies of the geodesic are now connected by $i - 2$ winding arches, with the rest of the quadrangulation in between. Upon continuous deformation on the sphere, we can recover the wanted zipper-like structure with the former winding arches now lying in between the two paths (see figure 5). This last structure is eventually zipped so as to recover the marked geodesic on the quadrangulation.

Now we see that, in the last transformation, it is crucial that the two copies of the geodesic path obtained by the inverse construction have no common vertex (except for their first and last vertices). This is the case for a spine tree resulting from the modified Schaeffer's construction on a quadrangulation with a marked geodesic, but this is not true in general for an arbitrary spine tree. Indeed, for an arbitrary spine tree, it may happen that the successor of a corner on the right of the spine lies itself on the spine (see figure 6), necessarily on its left side. If so, we will obtain two geodesic paths with a common vertex acting as a *pinch point* separating the rest of the quadrangulation into two parts (see figure 6).

When applying the inverse construction to a general well-labeled spine tree with spine of length $i - 1$, if we decide not to draw the winding arches, the most general object that we end up with is a *quadrangulation with a geodesic boundary* of length $2i$, i.e. a boundary with a
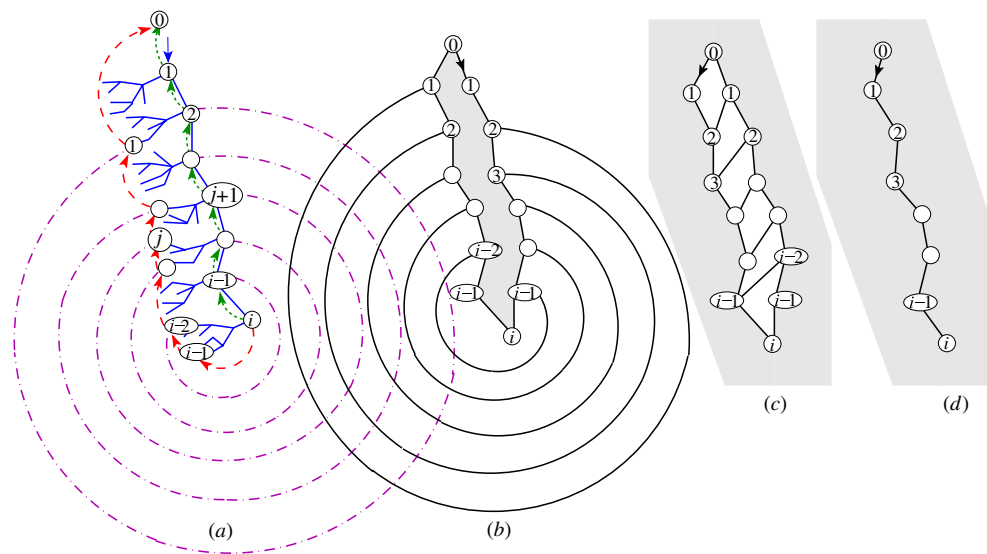
Figure 5. Starting from a spine tree obtained as in figure 4, we reconstruct the two copies of the geodesic path by linking corners to their successors (a). Corners on the left of the spine create the first copy (green short-dashed arches), while the chain of successors of the vertex i at the end of the spine creates the other copy (red long-dashed arches), the two copies being connected by winding (magenta dot-dashed) arches. They moreover surround all subtrees hanging from the spine hence, after completing the inverse construction, serve as boundaries for the rest of the quadrangulation (grey background in (b)). On the sphere, this configuration can be deformed into a quadrangulation with an internal zipper-like structure (c) which can be eventually squeezed into a marked geodesic (d).

marked origin vertex and such that the two paths of length i joining this origin to its antipodal vertex are geodesic paths (see figure 7 for an illustration). This requirement is equivalent to demanding that the vertex antipodal to the origin be indeed at distance i from this origin in the whole quadrangulation, i.e. all paths in the bulk of the quadrangulation from the origin to that vertex have lengths larger than or equal to i. The two geodesic paths forming the boundary may however meet at common vertices (with necessarily the same label on both sides) or even along common edges. The construction above is clearly one-to-one.

This constitutes *bijection I* between, on the one hand, quadrangulations with a geodesic boundary of length $2i$ (and possibly pinch points) and, on the other hand, planted well-labeled spine trees with spine of length $i - 1$. By convention, for $i = 1$, a well-labeled spine tree with spine of length 0 is nothing but a well-labeled tree planted at a corner labeled 1.

Moreover, there is a straightforward *bijection II* between quadrangulations with a geodesic boundary of length $2i$ *having no pinch point* and quadrangulations with a marked geodesic of length i, as obtained by gluing the two sides of the boundary around the sphere (see figure 7).

We could easily characterize the subset of spine trees which are in correspondence with geodesic boundaries without pinch points. It is however much simpler to note that a quadrangulation whose boundary has k pinch points and length $2i$ may be uniquely decomposed into $k + 1$ *irreducible components* whose boundary lengths add up to $2i$. Each of these irreducible components is either a single edge or is precisely a quadrangulation with a geodesic boundary having no pinch point. This constitutes *bijection III* and is the final step that will allow us to relate the enumeration of quadrangulations with a marked geodesic to that of spine trees.
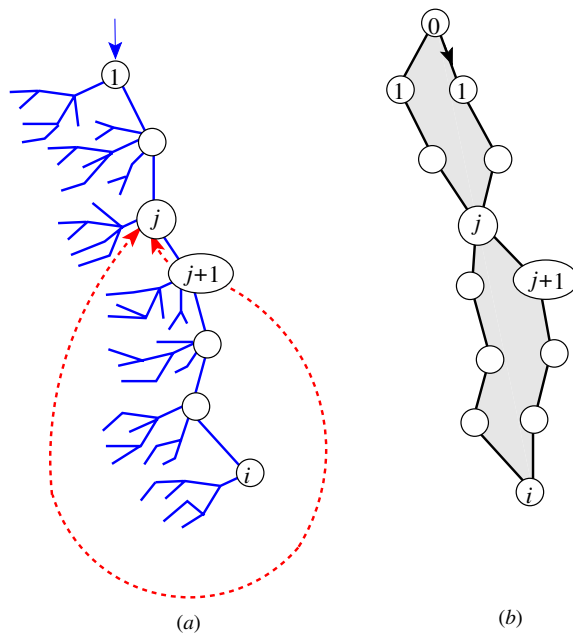
Figure 6. Appearance of pinch points in the inverse construction from a generic spine tree. If the successor of a corner labeled $j + 1$ on the right of the spine happens to be itself on the spine (*a*), this creates a pinch point at a distance j from the origin in the associated quadrangulation (*b*). Here we have not represented the winding arches, as opposed to figure 5.
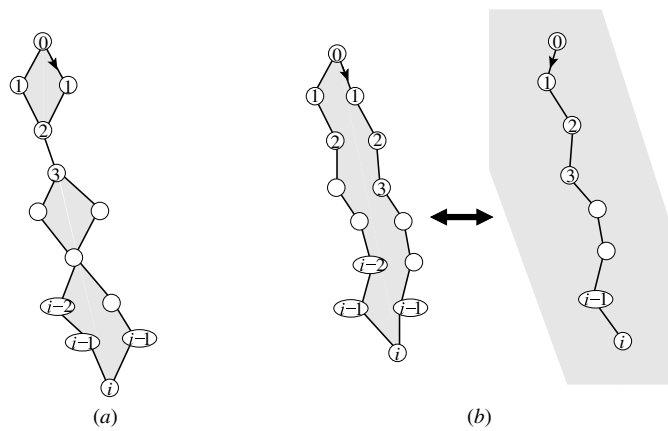
Figure 7. A schematic picture (*a*) of a quadrangulation with a geodesic boundary of length $2i$, as obtained from the inverse construction acting on a generic spine tree. The two geodesic paths bounding the quadrangulation may have pinch points in the form of common vertices and/or common edges. Quadrangulations with a geodesic boundary of length $2i$ having no pinch point (*b*) are in bijection with quadrangulations with a marked geodesic of length i.

2.3. Generating functions

We would now like to count quadrangulations with marked geodesics. As usual, we will consider the generating function of such maps with a weight g per face. In the well-labeled tree language, this translates into a weight g per edge of the tree. We shall call $R_i(g)$ the generating function for well-labeled trees planted at a corner labeled i. From Schaeffer's bijection, $R_1(g)$ is nothing but the generating function of rooted planar quadrangulations or planar quadrangulations with a marked geodesic of length 1. As mentioned in [9], it can be shown that the quantity $\log(R_i(g)/R_{i-1}(g))$ is the generating function for quadrangulations with two marked (and distinguished) vertices at distance i from each other (counted with symmetry factors). The generating functions $R_i(g)$ satisfy the recursion relations

$$R_i(g) = \frac{1}{1 - g(R_{i-1}(g) + R_i(g) + R_{i+1}(g))} \tag{2.1}$$

for $i \geqslant 1$ with the convention $R_0 = 0$. This relation simply states that a well-labeled tree planted at a vertex labeled i is formed by a collection of an arbitrary number of subtrees hanging from that vertex which are themselves well-labeled trees with a root vertex labeled $i - 1, i$ or $i + 1$. These recursion relations were solved in [11], with the result

$$R_i(g) = R(g) \frac{(1 - x(g)^i)(1 - x(g)^{i+3})}{(1 - x(g)^{i+1})(1 - x(g)^{i+2})}, \qquad \text{where}$$

$$R(g) = \frac{1 - \sqrt{1 - 12g}}{6g} \qquad \text{and} \tag{2.2}$$

$$x(g) = \frac{1 - 24g - \sqrt{1 - 12g} + \sqrt{6}\sqrt{72g^2 + 6g + \sqrt{1 - 12g} - 1}}{2(6g + \sqrt{1 - 12g} - 1)}.$$

In this expression, the functions $R(g)$ and $x(g)$ are explicit solutions of the equations

$$R(g) = 1 + 3g(R(g))^2, \qquad x(g) + \frac{1}{x(g)} + 1 = \frac{1}{g(R(g))^2}. \tag{2.3}$$

All functions above have a singularity at $g = g_{\text{crit}} = 1/12$, which governs the asymptotic behavior of the general term in their series expansions in g. From $R_i(g)$, it is easy to obtain the generating function $Z_i(g)$ for well-labeled spine trees with a spine of length $i - 1$ as these trees are simply made of a spine with i attached well-labeled subtrees whose root vertices have labels increasing from 1 to i. We immediately get

$$Z_i(g) = \prod_{j=1}^{i} R_j(g) = R(g)^i \frac{(1 - x(g))(1 - x(g)^{i+3})}{(1 - x(g)^3)(1 - x(g)^{i+1})}. \tag{2.4}$$

For convenience, we decided not to assign the weight g to the edges of the spine. Indeed, in our construction, these edges correspond to the added squares which were not present in the original quadrangulation, and should therefore not be counted as real squares. From bijection I of the previous section, $Z_i(g)$ is nothing but the generating function of quadrangulations with a geodesic boundary of length $2i$, as defined above. For instance, we have the expansion $Z_2(g) = 1 + 5g + 32g^2 + 234g^3 + \cdots$, where the first two terms correspond to the configurations displayed in figure 8.

Finally, we will denote by $U_i(g)$ the generating function of quadrangulations with a geodesic boundary of length $2i$ made of two geodesic paths that have no pinch point. As we have seen, from bijection II, $U_i(g)$ is precisely the desired generating function for quadrangulations with a marked geodesic of length i. From bijection III, the function $U_i(g)$ is
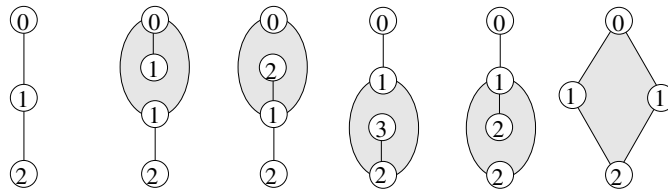
Figure 8. The set of all quadrangulations with a geodesic boundary of length 4 and with zero or one face (in grey).
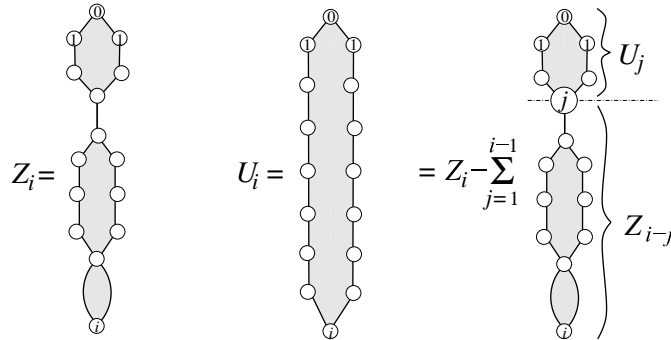

Figure 9. A schematic picture of the configurations of quadrangulations with a geodesic boundary of length $2i$ as counted by Z_i (the generic case) or U_i (the case with no pinch point), and of their relation (2.5).

nothing but the irreducible part of $Z_i(g)$ obtained inductively via the relation

$$U_1(g) = Z_1(g) = R_1(g), \qquad U_i(g) = Z_i(g) - \sum_{j=1}^{i-1} U_j(g) Z_{i-j}(g), \qquad i \geqslant 2. \qquad (2.5)$$

The subtraction term simply amounts to removing those quadrangulations for which the two geodesic paths have their closest pinch point to the origin at distance j, dividing the quadrangulation into a first irreducible part ($U_j(g)$) and the remaining part with possibly other pinch points ($Z_{i-j}(g)$), as illustrated in figure 9. For instance, we have $U_2(g) = g + 10g^2 + 90g^3 + 810g^4 + \cdots$, where the first two terms correspond to the configurations of figure 10 of quadrangulations with a geodesic boundary of length 4 having no pinch point, or equivalently, to the configurations of figure 11 of quadrangulations with a marked geodesic of length 2.

2.4. Confluent geodesics

With the above generating functions at hand, we have also access to generating functions for quadrangulations with several marked confluent geodesics, namely, quadrangulations with say, k marked geodesic paths joining a common origin vertex to a common endpoint at distance i. We shall furthermore impose that these k geodesics be weakly avoiding, in the sense that they *do not cross each other*, but still can have common vertices or even common edges. We shall also consider the case of strongly avoiding confluent geodesics which are required to have no common vertex except for their first and last endpoints. In both cases, we furthermore decide to distinguish one of the geodesics as the first one, which induces a natural linear ordering of the geodesics.
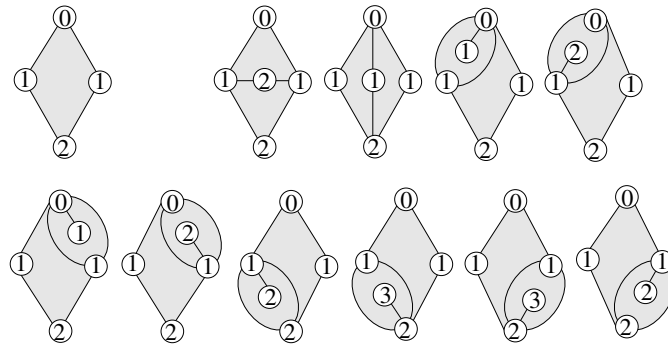
Figure 10. The set of all quadrangulations with a geodesic boundary of length 4 having no pinch point, with one or two faces (in grey).
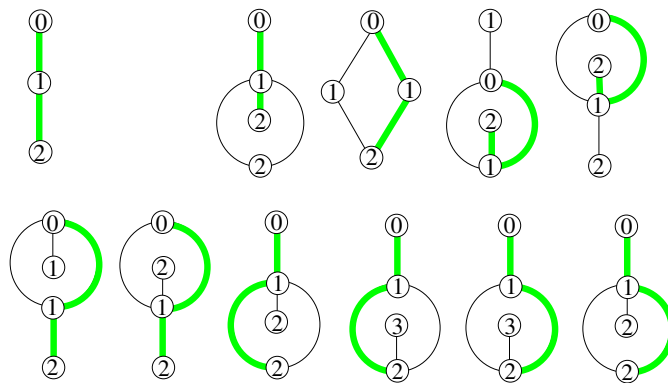

Figure 11. The set of all quadrangulations of the sphere with a marked geodesic (thick line) of length 2 and with one or two faces. These configurations are in one-to-one correspondence with those of figure 10. When drawing the quadrangulation in the plane, we choose as external face the one lying on the left of the $0 \to 1$ edge of the geodesic path.

Now a quadrangulation with k such linearly ordered weakly avoiding geodesics may be transformed upon unzipping of the first geodesic and continuous deformation on the sphere into a quadrangulations with a geodesic boundary and $k-1$ marked geodesics in the bulk of the quadrangulation (see figure 12). Note that these geodesics may very well have common vertices or edges among themselves and with the boundary if the corresponding geodesics had such common vertices or edges on the quadrangulation. Nevertheless, there is a global requirement that the two boundaries themselves cannot have common vertices. Without this requirement, the generating function would simply be $(Z_i(g))^k$ by viewing the configuration as simply made of k glued objects counted by $Z_i(g)$. To account for the global constraint, we again simply have to extract the irreducible part of $(Z_i(g))^k$, leading to a generating function $U_i^{(k)}(g)$ for quadrangulations with k marked weakly avoiding confluent geodesics of length i given by

$$U_1^{(k)}(g) = (Z_1(g))^k,$$

$$U_i^{(k)}(g) = (Z_i(g))^k - \sum_{j=1}^{i-1} U_j^{(k)}(g)(Z_{i-j}(g))^k, \qquad i \geqslant 2. \tag{2.6}$$
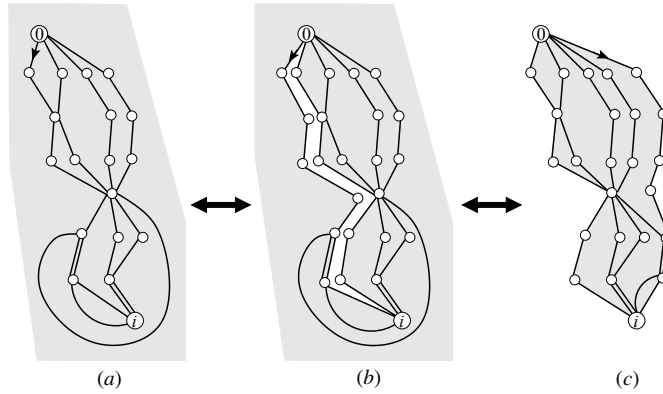
11

Figure 12. Schematic picture of a configuration (*a*) with *k* weakly avoiding confluent geodesics (here *k* = 4). Upon unzipping (*b*) of the first geodesic path (here marked by an arrow) and continuous deformation on the sphere, we end up with a quadrangulation with a geodesic boundary (*c*) and *k* − 1 geodesics in the bulk. It can be viewed as the juxtaposition of *k* quadrangulations with boundary of the type depicted in figure 7(*a*) with the global constraint that the two outermost boundaries cannot have common vertices.

Finally, the situation is even simpler in the case of *k* strongly avoiding geodesics since in this case, upon unzipping all geodesics, we obtain exactly *k* quadrangulations with a geodesic boundary with no pinch point. The generating function $\tilde{U}_i^{(k)}(g)$ for quadrangulations with *k* marked strongly avoiding geodesics of length *i* is therefore given by

$$\tilde{U}_i^{(k)}(g) = (U_i(g))^k. \tag{2.7}$$

3. Statistics of geodesics in large quadrangulations

3.1. From combinatorics to statistics

Let us now see how to use the above generating functions to study the statistics of geodesics in quadrangulations. We shall be interested in averaging over all quadrangulations with a *fixed number n* of faces. As customary, our enumeration results translate naturally into averages for an ensemble where every quadrangulation is drawn with a probability proportional to its *inverse symmetry factor*, i.e. to the inverse of the order of its automorphism group. In the limit $n \to \infty$ of large quadrangulations, it is expected that the symmetry factors become irrelevant, so that the asymptotic statistics is the same as for the uniform probability distribution.

In our case, a natural quantity to look at is the number of geodesics emerging from a given origin. In this context, it is natural to consider the ensemble of *pointed quadrangulations* with *n* faces, i.e. quadrangulations with a marked origin vertex, again weighted by their inverse symmetry factor. The probability of a given pointed quadrangulation is then equal to $1/(S\mathcal{Z}_n)$, where *S* is the symmetry factor and $\mathcal{Z}_n$ is the partition function, which reads

$$\mathcal{Z}_n = \frac{3^n}{2n} \frac{\binom{2n}{n}}{n+1}. \tag{3.1}$$

For instance, for *n* = 1 and 2, the results $\mathcal{Z}_1 = 3/2$ and $\mathcal{Z}_2 = 9/2$ are illustrated in figure 13. Note that, in contrast with rooted quadrangulations, pointed quadrangulations may have non-trivial symmetries, hence $\mathcal{Z}_n$ is not necessarily an integer.

In this ensemble, we can interpret the quantity $U_i(g)|_{g^n}/\mathcal{Z}_n$ as the average number of geodesics of length *i* emerging from the origin. For *i* = 2, we have $U_2(g) = g + 10 g^2 + \cdots$,
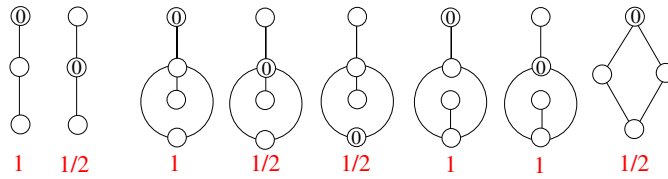
Figure 13. The set of all pointed quadrangulations of the sphere with one and two faces, where we have indicated the marked vertex by a label 0. For each configuration, we indicated its inverse symmetry factor. These add up to $\mathcal{Z}_1 = 3/2$ for one face and to $\mathcal{Z}_2 = 9/2$ for two faces.
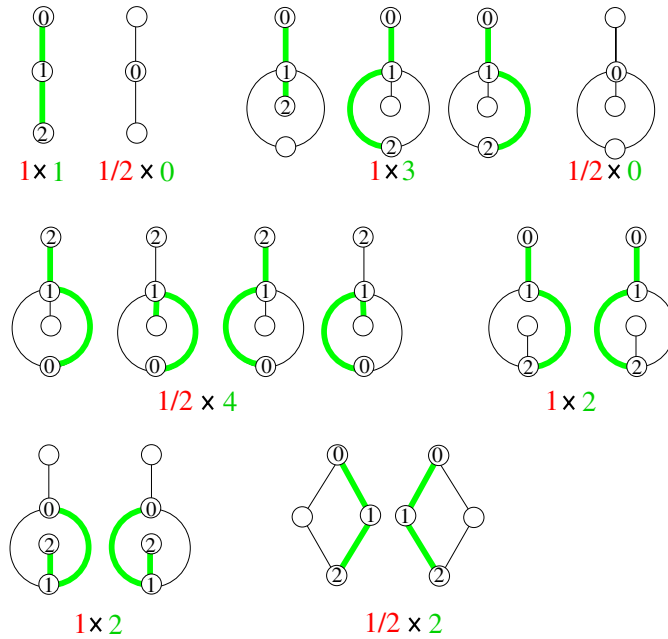

Figure 14. The average number of geodesics of length 2 emerging from the origin of pointed quadrangulations with one and two faces. This average is obtained as the sum over pointed quadrangulations of the actual number of geodesics (indicated in green on the right) times the symmetry factor of figure 13 (indicated in red on the left), leading to 1 (for $n = 1$) and 10 (for $n = 2$), and dividing by the partition function.

so that, for $n = 1$ and 2, this average number reads, respectively, $1/(3/2) = 2/3$ and $10/(9/2) = 20/9$ (see figure 14 for an illustration).

Alternatively, we can be interested in the ensemble of quadrangulations with two marked vertices at distance i from each other, again weighted by symmetry factors. In that case, as mentioned above, the partition function is known to be $\log(R_i(g)/R_{i-1}(g))|_{g^n}$. In this ensemble, the average number of geodesics joining the two marked points is simply $U_i(g)|_{g^n}$ divided by this different normalization.

3.2. Average number of geodesics in large quadrangulations

We are now interested in the large n limit of the statistics of geodesics. To this end, we first need to extract the coefficient of g^n in the various generating functions of the previous section.

For an arbitrary series $X(g)$, this coefficient is obtained via a contour integral around 0:

$$X(g)|_{g^n} = \frac{1}{2i\pi} \oint \frac{dg}{g^{n+1}} X(g). \tag{3.2}$$

In the case of our generating functions, the large n behavior is governed by their singularity at the critical value $g_{crit} = 1/12$. To capture this singularity, it is convenient to first perform a change of variable from g to $V = gR(g)$, with $R(g)$ as in equation (2.2), such that

$$g = g(V) \equiv V - 3V^2, \tag{3.3}$$

leading to

$$X(g)|_{g^n} = \frac{1}{2i\pi} \oint \frac{dV}{(V(1-3V))^{n+1}} (1-6V)X(g(V)). \tag{3.4}$$

At large n, the dominant behavior is given by the vicinity of saddle point at $V_{crit} = 1/6$. Writing

$$V = \frac{1}{6}\left(1 + i\frac{\xi}{n^{1/2}}\right), \tag{3.5}$$

the contour integral over V becomes at large n an integral over real values of ξ:

$$X(g)|_{g^n} = \frac{12^n}{i\pi n} \int_{-\infty}^{+\infty} d\xi\, \xi\, e^{-\xi^2} \left(1 + \frac{\xi^4 - 2\xi^2}{2n} + \mathcal{O}\left(\frac{1}{n^2}\right)\right) X\left(\frac{1}{12}\left(1 + \frac{\xi^2}{n}\right)\right). \tag{3.6}$$

For $X = Z_i$ or U_i, we will find an expansion of the form

$$X\left(\frac{1}{12}\left(1 + \frac{\xi^2}{n}\right)\right) = A + C\frac{\xi^2}{n} + \frac{2}{3}iD\frac{\xi^3}{n^{3/2}} + \mathcal{O}\left(\frac{1}{n^2}\right) \tag{3.7}$$

with real coefficients A, C and D, and with a vanishing $\xi/n^{1/2}$ term. We have introduced the prefactor 2/3 for later convenience. The even powers of ξ in (3.7) do not contribute to (3.6) by parity and we get the leading behavior

$$X(g)|_{g^n} \sim \frac{12^n}{\pi n} \int_{-\infty}^{+\infty} d\xi\, \frac{2}{3}D\frac{\xi^4}{n^{3/2}} e^{-\xi^2} = \frac{12^n}{2\sqrt{\pi}n^{5/2}} D. \tag{3.8}$$

As explained in the previous section, whenever $X(g)$ enumerates objects emerging from an origin, the corresponding average number $\langle x \rangle$ in the ensemble of pointed quadrangulations is obtained by dividing the above result by

$$\mathcal{Z}_n \sim \frac{12^n}{2\sqrt{\pi}n^{5/2}}, \tag{3.9}$$

so that the asymptotic average simply reads

$$\langle x \rangle = D. \tag{3.10}$$

Using the explicit form (2.4) for Z_i, we find immediately the expansion

$$Z_i = A_i + C_i\frac{\xi^2}{n} + \frac{2}{3}iD_i\frac{\xi^3}{n^{3/2}} + \cdots,$$

with
$$A_i = \frac{2^i(i+3)}{3(i+1)},$$

$$C_i = \frac{2^i i(i+3)(i^2+6i+3)}{30(i+1)}, \tag{3.11}$$

$$D_i = \frac{2^i i(i+2)(i+3)(i+4)(3i^2+12i+13)}{420(i+1)},$$

from which we obtain the large n asymptotic behavior

$$Z_i(g)|_{g^n} = \frac{12^n}{\sqrt{\pi}n^{5/2}} \frac{2^i i(i+2)(i+3)(i+4)(3i^2+12i+13)}{840(i+1)}. \tag{3.12}$$

As for U_i, we have a similar expansion

$$U_i = \alpha_i + \gamma_i \frac{\xi^2}{n} + \frac{2}{3}i\delta_i \frac{\xi^3}{n^{3/2}} + \cdots, \tag{3.13}$$

where the coefficient δ_i gives the large n behavior of U_i via the general relation (3.8). In particular, from (3.10), *the average number of geodesic paths of length i emerging from the origin vertex in the ensemble of pointed quadrangulations of fixed large size is directly given by δ_i.* The coefficients α_i, γ_i and δ_i can be related to A_i, C_i and D_i via relation (2.5), namely,

$$\alpha_i = A_i - \sum_{j=1}^{i-1}\alpha_j A_{i-j},$$

$$\gamma_i = C_i - \sum_{j=1}^{i-1}(\alpha_j C_{i-j} + \gamma_j A_{i-j}), \tag{3.14}$$

$$\delta_i = D_i - \sum_{j=1}^{i-1}(\alpha_j D_{i-j} + \delta_j A_{i-j}).$$

These relations are better expressed by introducing generating functions for these coefficients:

$$\hat{A}(t) \equiv \sum_{i=1}^{\infty} A_i t^i, \qquad \hat{C}(t) \equiv \sum_{i=1}^{\infty} C_i t^i, \qquad \hat{D}(t) \equiv \sum_{i=1}^{\infty} D_i t^i,$$

$$\hat{\alpha}(t) \equiv \sum_{i=1}^{\infty} \alpha_i t^i, \qquad \hat{\gamma}(t) \equiv \sum_{i=1}^{\infty} \gamma_i t^i, \qquad \hat{\delta}(t) \equiv \sum_{i=1}^{\infty} \delta_i t^i, \tag{3.15}$$

as they translate into

$$\hat{\alpha}(t) = \frac{\hat{A}(t)}{1+\hat{A}(t)}, \qquad \hat{\gamma}(t) = \frac{\hat{C}(t)}{(1+\hat{A}(t))^2}, \qquad \hat{\delta}(t) = \frac{\hat{D}(t)}{(1+\hat{A}(t))^2}. \tag{3.16}$$

From the explicit values of A_i, C_i and D_i, we can get explicit values for all these generating functions, leading to

$$\hat{\alpha}(t) = \frac{t(6t-2)-(1-2t)\log(1-2t)}{t-(1-2t)\log(1-2t)},$$

$$\hat{\gamma}(t) = \frac{3t(2t(20t^3-34t^2+17t-1)-(1-2t)^4\log(1-2t))}{5(1-2t)^2(t-(1-2t)\log(1-2t))^2},$$

$$\hat{\delta}(t) = \frac{3t(2t(3+177t-412t^2+708t^3-624t^4+224t^5)+3(1-2t)^6\log(1-2t))}{70(1-2t)^4(t-(1-2t)\log(1-2t))^2}$$

$$= 4t + \frac{80}{3}t^2 + 132t^3 + \frac{366\,208}{675}t^4 + \frac{3998\,176}{2025}t^5 + \mathcal{O}(t^6). \tag{3.17}$$

The function $\hat{\delta}(t)$ is the generating function for the average number δ_i of geodesics of length i emerging from the origin vertex in a large pointed quadrangulation. From the last line of (3.17), we directly read of the values of this average number for a length $i = 1, 2, \ldots, 5$.

We can easily estimate the large i behavior of α_i, γ_i and δ_i by looking at the singularity of $\hat{\alpha}(t)$, $\hat{\gamma}(t)$ and $\hat{\delta}(t)$ for $t \to 1/2$. Writing $t = 1/2(1 - \eta)$, we have the small η behavior:

$$\hat{\alpha}\left(\frac{1}{2}(1 - \eta)\right) = 1 - 3\eta - 6\eta^2 \log(\eta) + \cdots,$$

$$\hat{\gamma}\left(\frac{1}{2}(1 - \eta)\right) \sim \frac{9}{5\eta^2}, \tag{3.18}$$

$$\hat{\delta}\left(\frac{1}{2}(1 - \eta)\right) \sim \frac{54}{7\eta^4}.$$

Note that this last behavior follows immediately from the small η behaviors $\hat{A}(t) \sim 1/(3\eta)$ and $\hat{D}(t) \sim 6/(7\eta^6)$ and from relation (3.16). From (3.18), we deduce

$$\alpha_i \overset{i \to \infty}{\sim} 2^i \frac{12}{i^3}, \qquad \gamma_i \overset{i \to \infty}{\sim} 2^i \frac{9}{5} i, \qquad \delta_i \overset{i \to \infty}{\sim} 2^i \frac{9}{7} i^3. \tag{3.19}$$

From the discussion of the previous section, to go to the ensemble of quadrangulations with two marked vertices at distance i, we simply have to gauge δ_i by the average number of points at distance i from the origin in large pointed quadrangulations. This number is given by $(3/7)i^3$ for large i (see, for instance, equation (5.2) in [9]), hence we deduce that the average number $\langle \mathcal{G} \rangle_i$ of geodesics joining two fixed points at distance i from each other is simply given by

$$\langle \mathcal{G} \rangle_i \sim 3 \times 2^i \tag{3.20}$$

at large i. The leading exponential i-dependence can be heuristically understood as follows: note that choosing a particular geodesic leading to a given vertex simply amounts, when going backwards from that vertex, to choose recursively, for each vertex at distance i a predecessor vertex at distance $i - 1$, until we eventually reach the distance 0. Now one can easily show that, for a vertex at distance $i \gg 1$ from the origin of a random quadrangulation, its average number of neighbors at distance $i - 1$ is 2. There are thus on average two choices for each of the i steps leading back to the origin, which explains the 2^i factor by neglecting correlations. The prefactor 3 precisely accounts for these correlations as well as for the finite i corrections to the asymptotic number of choices 2.

3.3. Average number of confluent geodesics

We can as well obtain the average number of k-tuples of (linearly ordered) weakly avoiding confluent geodesics of length i by considering the expansion

$$(Z_i)^k = A_i^{(k)} + C_i^{(k)} \frac{\xi^2}{n} + \frac{2}{3} i D_i^{(k)} \frac{\xi^3}{n^{3/2}} + \cdots, \qquad \text{with}$$

$$A_i^{(k)} = (A_i)^k, \tag{3.21}$$

$$C_i^{(k)} = k(A_i)^{k-1} C_i,$$

$$D_i^{(k)} = k(A_i)^{k-1} D_i,$$

where the coefficients A_i, C_i and D_i are given by equation (3.11). In particular, the generating functions $\hat{A}^{(k)}(t) \equiv \sum_{i \geqslant 1} A_i^{(k)} t^i$, $\hat{C}^{(k)}(t) \equiv \sum_{i \geqslant 1} C_i^{(k)} t^i$ and $\hat{D}^{(k)}(t) \equiv \sum_{i \geqslant 1} D_i^{(k)} t^i$ now have a singularity at $t = 1/2^k$.

Similarly, the function $U_i^{(k)}$ has the expansion

$$U_i^{(k)} = \alpha_i^{(k)} + \gamma_i^{(k)} \frac{\xi^2}{n} + \frac{2}{3} i \delta_i^{(k)} \frac{\xi^3}{n^{3/2}} + \cdots, \tag{3.22}$$

where, as before, the coefficients $\alpha_i^{(k)}$, $\gamma_i^{(k)}$ and $\delta_i^{(k)}$ are determined through their generating functions:

$$\hat{\alpha}^{(k)}(t) \equiv \sum_{i \geqslant 1} \alpha_i^{(k)} t^i = \frac{\hat{A}^{(k)}(t)}{1 + \hat{A}^{(k)}(t)},$$

$$\hat{\gamma}^{(k)}(t) \equiv \sum_{i \geqslant 1} \gamma_i^{(k)} t^i = \frac{\hat{C}^{(k)}(t)}{(1 + \hat{A}^{(k)}(t))^2}, \qquad (3.23)$$

$$\hat{\delta}^{(k)}(t) \equiv \sum_{i \geqslant 1} \delta_i^{(k)} t^i = \frac{\hat{D}^{(k)}(t)}{(1 + \hat{A}^{(k)}(t))^2}.$$

Writing $t = 1/2^k(1 - \eta)$ and expanding at small η, we now have the dominant behaviors $\hat{A}^{(k)}(t) \sim 1/(3^k \eta)$ and $\hat{D}^{(k)}(t) \sim 6k/(3^{k-1} 7\eta^6)$, leading directly to $\hat{\delta}^{(k)}(t) \sim (k3^{k-1}54)/(7\eta^4)$. From this singularity, we immediately deduce the large i behavior of $\delta_i^{(k)}$:

$$\delta_i^{(k)} \overset{i \to \infty}{\sim} (2^i)^k k 3^{k-1} \frac{9}{7} i^3, \qquad (3.24)$$

which gives the average number of k-tuples of (linearly ordered) weakly avoiding confluent geodesics of length i emerging from the origin of a large pointed quadrangulation. Again, when compared with the average number $(3/7)i^3$ of vertices at distance i from this origin, this gives an average number

$$\langle \mathcal{G}_k \rangle_i \sim k(3 \times 2^i)^k \qquad (3.25)$$

of such k-tuples between the two marked points in the ensemble of quadrangulations with a large fixed size and two marked points at distance i from each other.

Let us make a few remarks on this particularly simple result. First, the leading exponential i-dependence 2^{ik} is surprisingly the same as for k independent geodesics. One could have expected a reduction of the entropy factor due to the constraint of non-intersection between geodesics. Indeed, as we shall see later, weakly avoiding confluent geodesics have a number of contacts which is proportional to their length. This apparent paradox can be explained as follows: as before, we can estimate the number of geodesics by looking at them backwards and choosing recursively for each vertex at distance i one of its predecessors at distance $i - 1$. For a vertex visited by a single geodesic, this gives two choices on average as before. When a number ℓ of geodesics come in contact at a vertex with p predecessors, the number of choices is now $\binom{p+\ell-1}{\ell}$ (instead of p^ℓ for freely intersecting geodesics). Now the probability of having p predecessors for a vertex at a large distance from the origin can be easily shown to be $1/2^p$ (with p varying from 1 to ∞), leading to an average value $\langle \binom{p+\ell-1}{\ell} \rangle = 2^\ell$, i.e. the same contribution as if the ℓ geodesics were visiting independent vertices. In other words, the reduction of choices among predecessors due to non-intersection is exactly compensated by the effect of correlations for the number of predecessors at a given vertex.

Even more surprising, the sub-leading prefactor 3 in equation (3.20) is simply raised to its kth power as if the effect of small i corrections and correlations along the geodesics could be treated independently for each geodesic path. Finally, we have in equation (3.25) a global prefactor k which can be understood as a spontaneous symmetry breaking effect as follows: the k confluent geodesics are linearly ordered and any pair of neighboring geodesics encloses a particular domain of the quadrangulation, with k such domains. As we shall see, for quadrangulations with a large number n of faces, only one of these k domains contains most of the area of the quadrangulation, i.e. has a number of faces close to n, while all the other domains have an area negligible with respect to n at large n. There are precisely k choices for the domain in which most of the area will lie, hence the global prefactor k.
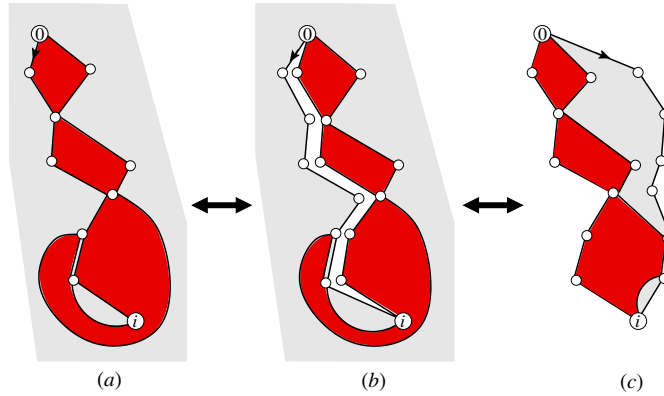
Figure 15. Schematic picture of a configuration (*a*) with two weakly avoiding confluent geodesics. The two geodesics delimit two (possibly disconnected) complementary domains (here in dark and light) lying between them. The same configuration (*c*) obtained upon unzipping of one geodesic path (*b*) and continuous deformation on the sphere.

3.4. Other statistical properties of confluent geodesics

By slight refinements of the above arguments, we have access to more involved statistical properties of confluent geodesics. For instance, we may compute the asymptotic (large n) average number $\langle c \rangle_i$ of contacts between two weakly avoiding confluent geodesics of length i, with result

$$\langle c \rangle_i \sim \frac{i}{3} \tag{3.26}$$

at large i. A proof of this result is presented in appendix A using the continuous formalism of section 4. As announced, this number is proportional to the length of the geodesics which indicates that the two geodesics 'stick' to one another.

Another quantity of interest is the area (number of faces) enclosed by these two geodesics. More precisely, let n_1 and n_2 be the areas of the two domains delimited by the geodesics in the quadrangulation, with $n_1 + n_2 = n$ (see figure 15 for an illustration). By symmetry, we have $\langle n_1 \rangle = \langle n_2 \rangle = n/2$ and a good measure of the dispatching of the area is given by the correlation $\langle n_1 n_2 \rangle$. For two geodesics of length i, we find

$$\langle n_1 n_2 \rangle_i \sim n \theta_i \tag{3.27}$$

for $n \to \infty$ and i finite, with a finite coefficient θ_i. This implies a very dissymmetric dispatching where the smaller domain has an average area of order θ_i only while almost all of the area lies in the larger domain. For large i, we obtained the leading behavior:

$$\theta_i \sim \tfrac{27}{100} i^3. \tag{3.28}$$

A derivation of this result is given in appendix B by use of the continuous framework of section 4. The above dissymmetry generalizes easily to the case of domains delimited by k confluent geodesics. We find that only one of these domains has an extensive area, meaning that the geodesics remain close to each other.

In view of the above results, we expect very different statistics for strongly avoiding confluent geodesics where contacts are forbidden. The asymptotic number of k-tuples of such

geodesics of length i is obtained from the expansion of $\tilde{U}_i^{(k)}$, namely,

$$
\begin{aligned}
\tilde{U}_i^{(k)} &= \tilde{\alpha}_i^{(k)} + \tilde{\gamma}_i^{(k)} \frac{\xi^2}{n} + \frac{2}{3} i \tilde{\delta}_i^{(k)} \frac{\xi^3}{n^{3/2}} + \cdots, \qquad \text{with} \\
\tilde{\alpha}_i^{(k)} &= (\alpha_i)^k, \\
\tilde{\gamma}_i^{(k)} &= k (\alpha_i)^{k-1} \gamma_i, \\
\tilde{\delta}_i^{(k)} &= k (\alpha_i)^{k-1} \delta_i.
\end{aligned}
\tag{3.29}
$$

From the large i behavior (3.19), we get

$$
\tilde{\delta}_i^{(k)} \overset{i \to \infty}{\sim} k(3 \times 2^i)^k \frac{3 \times 4^{k-1}}{7} i^{6-3k},
\tag{3.30}
$$

consisting of the same degeneracy factor $k(3 \times 2^i)^k$ as in equation (3.25) multiplied by a factor $(3 \times 4^{k-1}/7)i^{6-3k}$ which we interpret as counting the average number of vertices that are indeed reachable by k strongly avoiding geodesics. For $k > 2$, this factor goes to zero at large i, which indicates that distant vertices cannot be reached by more than two strongly avoiding geodesics. For $k = 2$, we have for each (large) value i of the distance an average number $12/7$ of vertices reachable from the origin by two strongly avoiding geodesics. We shall call such vertices *exceptional points*.

Let us now consider the areas n_1 and n_2 of the two domains delimited by two strongly avoiding confluent geodesics of length i. Again we want to compute the correlation $\langle n_1 n_2 \rangle$. This is done by considering the generating function $\left(g \frac{\mathrm{d}}{\mathrm{d}g} U_i(g) \right)^2$ as the action of $g \frac{\mathrm{d}}{\mathrm{d}g}$ amounts precisely to giving a weight proportional to the area. When going to the ξ variable, we have at leading order in n that $g \frac{\mathrm{d}}{\mathrm{d}g} = \frac{n}{2\xi} \frac{\mathrm{d}}{\mathrm{d}\xi}$ hence, from expansion (3.13), we get the expansion

$$
\left(g \frac{\mathrm{d}}{\mathrm{d}g} U_i(g) \right)^2 = \gamma_i^2 + 2i\gamma_i \delta_i \frac{\xi}{n^{1/2}} + \cdots.
\tag{3.31}
$$

Performing the integral over ξ, the first term vanishes by parity and we get the dominant behavior

$$
\left(g \frac{\mathrm{d}}{\mathrm{d}g} U_i(g) \right)^2 \Bigg|_{g^n} \sim \frac{12^n}{\sqrt{\pi} n^{3/2}} \gamma_i \delta_i.
\tag{3.32}
$$

This is to be compared with the asymptotic behavior

$$
(U_i(g))^2 |_{g^n} \sim \frac{12^n}{2\sqrt{\pi} n^{5/2}} \delta_i^{(2)} = \frac{12^n}{\sqrt{\pi} n^{5/2}} \alpha_i \delta_i.
\tag{3.33}
$$

Taking the ratio of (3.32) and (3.33), we get the asymptotic average

$$
\langle n_1 n_2 \rangle_i = n \frac{\gamma_i}{\alpha_i} \overset{i \to \infty}{\sim} \frac{3}{20} n i^4.
\tag{3.34}
$$

Again, almost all of the area is carried by a single domain, while the smaller domain now has an area of order i^4. This result is valid in the limit $n \to \infty$ and i finite but large. It will be extended in the following section to the scaling limit of large quadrangulations, which is obtained by taking $i \propto n^{1/4}$. In this limit, we have $i^4 \propto n$, which means that the smaller area is of the same order as the larger one, i.e. the two domains contain a finite fraction of the total area.
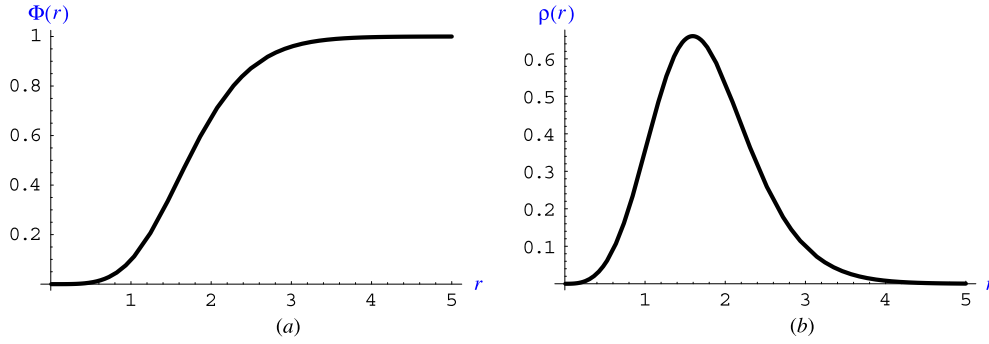
Figure 16. The distribution function $\Phi(r)$ measuring the probability that a vertex be at a rescaled distance less than r in the scaling limit of large quadrangulation. Its derivative $\rho(r)$ is the density of vertices at a rescaled distance r.

4. Continuum limit

4.1. Reminders

So far the results which we presented were obtained in the limit of a size n of the quadrangulations tending to infinity, keeping a finite value for the length i of the geodesics. On the other hand, it is well known that an interesting scaling limit may be obtained by letting both n and i tend to infinity, while keeping the ratio $i/n^{1/4}$ fixed.

As a reminder, let us first consider the average number of vertices within a ball of radius $i = rn^{1/4}$ centered at a given origin in a random quadrangulation of size n. In the limit $n \to \infty$, this average number behaves as $n\Phi(r)$, with $\Phi(r)$ a finite scaling function. This function was computed in [11], with the result

$$\Phi(r) = \frac{4}{\sqrt{\pi}} \int_0^\infty d\xi\, \xi^2\, e^{-\xi^2} \left(1 - 6\frac{1 - \cosh(r\sqrt{3\xi})\cos(r\sqrt{3\xi})}{(\cosh(r\sqrt{3\xi}) - \cos(r\sqrt{3\xi}))^2} \right). \qquad (4.1)$$

It increases from $\Phi(0) = 0$ to $\Phi(+\infty) = 1$ as it should and its derivative

$$\rho(r) \equiv \Phi'(r) \qquad (4.2)$$

may be interpreted as the average density of vertices at a rescaled distance r from a given origin. Both the functions $\Phi(r)$ and $\rho(r)$ are plotted in figure 16 for illustration. We have, in particular, the asymptotic behaviors:

$$\rho(r) \overset{r \to 0}{\sim} \tfrac{3}{7}r^3, \qquad \rho(r) \overset{r \to \infty}{\sim} e^{-3(3/8)^{2/3}r^{4/3}}. \qquad (4.3)$$

The rest of this section is devoted to the computation of similar scaling functions characterizing the statistics of geodesics in the same scaling limit.

4.2. Distribution of geodesics of length r

Let us first consider the case of quadrangulations of size n, with a single marked geodesic of length i, as counted by $U_i(g)|_{g^n}$. To estimate this quantity in the scaling limit, we first evaluate $Z_i(g)|_{g^n}$ from its explicit form (2.4). For $i = rn^{1/4}$, we have the expansion

$$\frac{1}{2^i} Z_i \left(\frac{1}{12} \left(1 + \frac{\xi^2}{n} \right) \right) = \frac{1}{3} + \frac{\mathcal{F}(r, \xi)}{n^{1/4}} + \mathcal{O}\left(\frac{1}{n^{1/2}} \right), \qquad \text{with}$$

$$\mathcal{F}(r, \xi) = \sqrt{-\frac{2}{3}\,\mathrm{i}\xi}\, \coth\left(r\sqrt{-\frac{3}{2}\,\mathrm{i}\xi} \right) + \frac{\mathrm{i}r\xi}{3}, \qquad (4.4)$$

which, upon substituting in (3.6), gives the asymptotic behavior

$$\left.\frac{Z_i}{2^i}\right|_{g^n} \overset{n\to\infty}{\sim} \frac{12^n}{\pi n^{5/4}} \int_0^\infty d\xi\, \xi\, e^{-\xi^2} \left(\frac{2r\xi}{3} - 2\sqrt{\frac{\xi}{3}}\frac{\sinh(r\sqrt{3\xi}) - \sin(r\sqrt{3\xi})}{\cosh(r\sqrt{3\xi}) - \cos(r\sqrt{3\xi})}\right). \tag{4.5}$$

In particular, for $r \to 0$, the integral behaves as $\sqrt{\pi} r^5/280$, leading to $(Z_i/2^i) \sim 12^n/$ $(\sqrt{\pi} n^{5/4}) \times (r^5/280)$, consistent with equation (3.12) in the regime $1 \ll i \ll n^{1/4}$.

As before, we may obtain U_i from Z_i via equation (2.5), which we rewrite as

$$\hat{U}(t) = \frac{\hat{Z}(t)}{1 + \hat{Z}(t)} \tag{4.6}$$

upon introducing the generating functions

$$\hat{Z}(t) \equiv \sum_{i=1}^\infty Z_i t^i, \qquad \hat{U}(t) \equiv \sum_{i=1}^\infty U_i t^i, \tag{4.7}$$

with a weight t per geodesic step. The scaling limit $i \propto n^{1/4} \to \infty$ is now captured by taking

$$t = \tfrac{1}{2} e^{-sn^{-1/4}}. \tag{4.8}$$

In this regime, we cannot simply plug the asymptotic form (4.4) of Z_i in $\hat{Z}(t)$ as $\mathcal{F}(r, \xi)$ has a pole at $r = 0$. A simple way to work around this problem is to subtract from Z_i its critical value $Z_i(1/12) = A_i$, as defined in section 3.2, and to write

$$(Z_i - A_i)t^i = \frac{e^{-sr}}{n^{1/4}}\left(\mathcal{F}(r, \xi) - \frac{2}{3r}\right) + \mathcal{O}\left(\frac{1}{n^{1/2}}\right). \tag{4.9}$$

Noting that the right hand side has no more pole, the sum over i can be approximated by an integral over r, leading to

$$\hat{Z}(t) - \hat{A}(t) = \int_0^\infty dr\, e^{-sr}\left(\mathcal{F}(r, \xi) - \frac{2}{3r}\right) + \mathcal{O}\left(\frac{1}{n^{1/4}}\right), \tag{4.10}$$

with, as before, $\hat{A}(t) = \sum A_i t^i$. From the explicit form (3.11), we find the explicit expansion of $\hat{A}(t)$:

$$\hat{A}(t) = \frac{n^{1/4}}{3s} - \frac{2}{3}\log\left(\frac{s}{n^{1/4}}\right) - \frac{5}{6} + \mathcal{O}\left(\frac{1}{n^{1/4}}\right). \tag{4.11}$$

Plugging these expansions into (4.6), we deduce the expansion of $\hat{U}(t)$:

$$\hat{U}(t) = 1 - \frac{3s}{n^{1/4}} + \frac{s^2}{n^{1/2}}\left(-6\log\left(\frac{s}{n^{1/4}}\right) + \frac{3}{2} + 9\int_0^\infty dr\, e^{-sr}\left(\mathcal{F}(r, \xi) - \frac{2}{3r}\right)\right) + \cdots$$

$$= \hat{\alpha}(t) + \frac{1}{n^{1/2}}\int_0^\infty dr\, e^{-sr}\left(9\mathcal{F}''(r, \xi) - \frac{12}{r^3}\right) + \cdots, \tag{4.12}$$

where we have identified the expansion of $\hat{\alpha}(t)$, as defined in section 3.2, and with $\mathcal{F}'' \equiv \partial^2\mathcal{F}/\partial r^2$. Going back to $U_i(g)$, this gives an expansion

$$\frac{1}{2^i}(U_i - \alpha_i) = \frac{1}{n^{3/4}}\left(9\mathcal{F}''(r, \xi) - \frac{12}{r^3}\right) + \mathcal{O}\left(\frac{1}{n}\right), \tag{4.13}$$

which, from the asymptotics $\alpha_i \sim 12/i^3$ of equation (3.19), yields the scaling form

$$\frac{1}{2^i}U_i\left(\frac{1}{12}\left(1 + \frac{\xi^2}{n}\right)\right) = \frac{9\mathcal{F}''(r, \xi)}{n^{3/4}} + \mathcal{O}\left(\frac{1}{n}\right). \tag{4.14}$$

Surprisingly, when comparing with equation (4.4), we see that, in the scaling limit, extracting the irreducible part simply amounts to differentiating twice with respect to r. Upon substitution of (4.14) into equation (3.6), we obtain the desired asymptotic scaling behavior

$$\left. \frac{U_i}{2^i} \right|_{g^n} \overset{n\to\infty}{\sim} \frac{12^n}{\pi n^{7/4}} 9 \frac{\partial^2}{\partial r^2} \left\{ \int_0^\infty d\xi\, \xi\, e^{-\xi^2} \left(\frac{2r\xi}{3} - 2\sqrt{\frac{\xi}{3}} \frac{\sinh(r\sqrt{3\xi}) - \sin(r\sqrt{3\xi})}{\cosh(r\sqrt{3\xi}) - \cos(r\sqrt{3\xi})} \right) \right\}$$

$$= \frac{12^n}{2\sqrt{\pi} n^{7/4}} \times 3\Phi'(r) = \frac{12^n}{2\sqrt{\pi} n^{7/4}} \times 3\rho(r). \tag{4.15}$$

Up to a factor of 3, this last expression is nothing but the number of quadrangulations with simply a marked vertex at distance $i = rn^{1/4}$ from a given origin. We therefore recover in the scaling limit the same ratio 3×2^i as obtained in equation (3.20) for $1 \ll i \ll n^{1/4}$ between geodesics of length i and vertices at distance i. Up to this degeneracy factor, the density of geodesics of rescaled length r coincides with the density of vertices at distance r.

We can easily play the same game with k-tuples of weakly confluent geodesics. Using the expansion

$$\frac{1}{(2^i)^k} \left(Z_i^k - A_i^{(k)} \right) = \frac{k}{3^{k-1}} \frac{1}{n^{1/4}} \left(\mathcal{F}(r, \xi) - \frac{2}{3r} \right) + \mathcal{O}\left(\frac{1}{n^{1/2}} \right), \tag{4.16}$$

we now get, for $t = e^{-sn^{-1/4}}/2^k$,

$$\hat{U}^{(k)}(t) = \hat{\alpha}^{(k)}(t) + \frac{k 3^{k+1}}{n^{1/2}} \int_0^\infty dr\, e^{-sr} \left(\mathcal{F}''(r, \xi) - \frac{4}{3r^3} \right) + \mathcal{O}\left(\frac{1}{n^{3/4}} \right), \tag{4.17}$$

leading to

$$\left. \frac{U_i^{(k)}}{(2^i)^k} \right|_{g^n} \overset{n\to\infty}{\sim} \frac{12^n}{2\sqrt{\pi} n^{7/4}} k 3^k \rho(r). \tag{4.18}$$

Again, in the scaling limit, the density of k-tuples of weakly avoiding confluent geodesics of length r coincides with the density $\rho(r)$ upon a simple renormalization by a degeneracy factor $k(3 \times 2^i)^k$, in agreement with equation (3.25).

In the case $k = 2$ and by a slight refinement of our generating functions, we may compute the average number of contacts between two weakly avoiding confluent geodesics of rescaled length r. This calculation is detailed in appendix A, with the result

$$\langle c \rangle_r = n^{1/4} \frac{r}{3}, \tag{4.19}$$

which extends the finite i linear dependence displayed in equation (3.26) to the whole range of r in the scaling regime.

4.3. Exceptional points

The situation is more interesting for exceptional points as it will lead us to a new scaling function. We consider again the case of two strongly avoiding confluent geodesics of length i, as counted by U_i^2. From equation (4.14), we now get for $i = rn^{1/4}$ the scaling behavior

$$\left. \frac{(U_i)^2}{(2^i)^2} \right|_{g^n} \overset{n\to\infty}{\sim} \frac{12^n}{i\pi n^{5/2}} \int_{-\infty}^{+\infty} d\xi\, \xi\, e^{-\xi^2} (9\mathcal{F}''(r,\xi))^2 = \frac{12^n}{2\sqrt{\pi} n^{5/2}} (2 \times 3^2) \sigma(r), \tag{4.20}$$

where

$$\sigma(r) \equiv \frac{432}{\sqrt{\pi}} \int_0^\infty d\xi\, \xi^4\, e^{-\xi^2} \left\{ 8 \frac{(c\tilde{c}-1)^3}{(c-\tilde{c})^6} + 2 \frac{(c\tilde{c}-1)(c\tilde{c}-4)}{(c-\tilde{c})^4} - \frac{1}{(c-\tilde{c})^2} \right\}, \tag{4.21}$$

with $\qquad c \equiv \cosh(r\sqrt{3\xi}), \qquad \tilde{c} \equiv \cos(r\sqrt{3\xi}).$
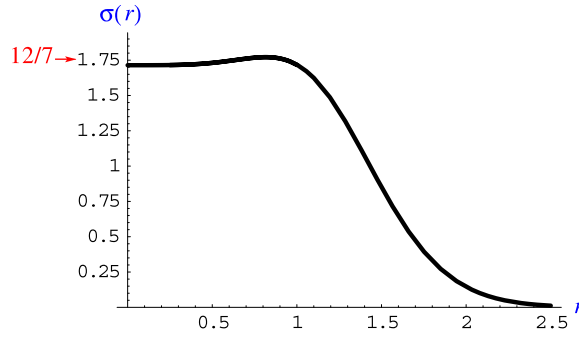
Figure 17. The scaling function $\sigma(r)$ counting the number of exceptional points at a rescaled distance r form the origin in the scaling limit of large quadrangulations. There are on average $n^{1/4}\sigma(r)\,\mathrm{d}r$ such exceptional points at a rescaled distance between r and $r + \mathrm{d}r$.

We have factored out in equation (4.20) the asymptotic number $12^n/(2\sqrt{\pi}n^{5/2})$ of quadrangulations with a given origin as well as a degeneracy factor 2×3^2 for two confluent geodesics. We may then interpret the remaining finite scaling function $\sigma(r)$ as counting the number of exceptional points at a rescaled distance r from a given origin. This function is plotted in figure 17 and has the following limiting behaviors:

$$\sigma(r) \overset{r\to 0}{\to} 12/7, \qquad \sigma(r) \overset{r\to\infty}{\sim} e^{-3(3/2)^{2/3}r^{4/3}}. \tag{4.22}$$

Note that the small r limit corroborates the finite i result of section 3.4. Finally, upon summing over i, the total number of exceptional points is simply given by $n^{1/4}\int_0^\infty \mathrm{d}r\,\sigma(r)$.

4.4. Area between two geodesics

Let us finally address again the question of the dispatching of the area between geodesics, now in the scaling limit. Considering two non-intersecting geodesics, we shall call ω_1 and ω_2 the fraction of the total area n carried by the two domains which they separate, with of course $\omega_1 + \omega_2 = 1$. A convenient way to access the average properties of ω_1 and ω_2 is to introduce extra weight parameters λ_1 and λ_2 coupled to the area of the two domains. In the case of weakly avoiding geodesics, we therefore consider the refined generating function $Z_i(\lambda_1 g)Z_i(\lambda_2 g)$ counting quadrangulations with a weight $\lambda_1 g$ (respectively $\lambda_2 g$) per square in the first (respectively second) domain. Now we may explore the scaling limit of $Z_i(\lambda_1 g)Z_i(\lambda_2 g)$ by taking $\lambda_i = 1 + \mathcal{O}(1/n)$, namely, by writing

$$
\begin{aligned}
g &= \frac{1}{12}\left(1 + \frac{\xi^2}{n}\right), \\
\lambda_1 g &= \frac{1}{12}\left(1 + \frac{\mu_1^2}{n}\right) + \mathcal{O}\left(\frac{1}{n^2}\right), \\
\lambda_2 g &= \frac{1}{12}\left(1 + \frac{\mu_2^2}{n}\right) + \mathcal{O}\left(\frac{1}{n^2}\right),
\end{aligned}
\tag{4.23}
$$

with $\mu_i \equiv \mu_i(\lambda_i, \xi)$ such that $\mu_i(1, \xi) = \xi$. At large n and for $i = rn^{1/4}$, we have the expansion:

$$\frac{1}{(2^i)^2}Z_i(\lambda_1 g)Z_i(\lambda_2 g) = \frac{1}{3^2} + \frac{\mathcal{F}(r, \mu_1) + \mathcal{F}(r, \mu_2)}{3n^{1/4}} + \mathcal{O}\left(\frac{1}{n^{1/2}}\right). \tag{4.24}$$

Taking the corresponding irreducible part leads to a generating function $U_i^{(2)}(g; \lambda_1, \lambda_2)$ with expansion

$$\frac{1}{(2^i)^2} U_i^{(2)}(g; \lambda_1, \lambda_2) = \frac{27(\mathcal{F}''(r, \mu_1) + \mathcal{F}''(r, \mu_2))}{n^{3/4}} + \mathcal{O}\left(\frac{1}{n}\right), \qquad (4.25)$$

and we end up with

$$\frac{U_i^{(2)}(g; \lambda_1, \lambda_2)}{(2^i)^2}\bigg|_{g^n} \overset{n\to\infty}{\sim} \frac{12^n}{\pi n^{7/4}} 27 \int_{-\infty}^{+\infty} d\xi\, e^{-\xi^2} \{\mathcal{F}''(r, \mu_1) + \mathcal{F}''(r, \mu_2)\}. \qquad (4.26)$$

To extract $\langle \omega_i \rangle$ ($i = 1, 2$), we must apply the operator $(\lambda_i/n)(\partial/\partial\lambda_i)$ and let $\lambda_i \to 1$, i.e. $\mu_i \to \xi$. At leading order in n, we have $(\lambda_i/n)(\partial/\partial\lambda_i) = 1/(2\mu_i)(\partial/\partial\mu_i)$ and we thus get

$$\langle \omega_1 \rangle_r = \langle \omega_2 \rangle_r = \frac{\int_{-\infty}^{+\infty} d\xi\, \xi\, e^{-\xi^2} \frac{1}{2\xi} \frac{\partial}{\partial\xi} \mathcal{F}''(r, \xi)}{\int_{-\infty}^{+\infty} d\xi\, \xi\, e^{-\xi^2} 2\mathcal{F}''(r, \xi)} = \frac{1}{2} \qquad (4.27)$$

as seen by an integration by part. This average result simply expresses the symmetry between the two domains and does not tell us anything about the actual dispatching of the area. As before, this dispatching is better measured by the correlation $\langle \omega_1 \omega_2 \rangle$. This latter average requires the action of the operator $1/(4\mu_1\mu_2)\partial^2/\partial\mu_1\partial\mu_2$ on the integrand in (4.26), which produces a vanishing result, namely,

$$\langle \omega_1 \omega_2 \rangle_r = 0 \qquad (4.28)$$

in the limit $n \to \infty$. In other words, the fraction of the area of the smaller domain tends to 0 at large n. A closer look at the corrections to scaling leads to $\langle \omega_1 \omega_2 \rangle_r = \mathcal{O}(1/n^{1/4})$, with an r-dependent coefficient. An integral formula for this coefficient is presented in appendix B. In particular, for small r, it behaves as $27r^3/100$, which is precisely the result announced in equation (3.28) when $i = rn^{1/4}$.

This situation is to be contrasted with the case of two strongly avoiding geodesics, for which we must consider directly the expansion of $U_i(\lambda_1 g)U_i(\lambda_2 g)$, namely,

$$\frac{1}{(2^i)^2} U_i(\lambda_1 g)U_i(\lambda_2 g)\bigg|_{g^n} = \frac{12^n}{i\pi n^{5/2}} \int_{-\infty}^{+\infty} d\xi\, \xi\, e^{-\xi^2} 81\mathcal{F}''(r, \mu_1)\mathcal{F}''(r, \mu_2). \qquad (4.29)$$

Applying again $1/(2\mu_i)\partial/\partial\mu_i$, we recover $\langle \omega_1 \rangle_r = \langle \omega_2 \rangle_r = 1/2$, while we now obtain

$$\langle \omega_1 \omega_2 \rangle_r = \frac{\int_{-\infty}^{+\infty} d\xi\, \xi\, e^{-\xi^2} \left(\frac{1}{2\xi}\frac{\partial\mathcal{F}''}{\partial\xi}(r, \xi)\right)^2}{\int_{-\infty}^{+\infty} d\xi\, \xi\, e^{-\xi^2} (\mathcal{F}''(r, \xi))^2} = \frac{\lambda(r)}{\sigma(r)}, \qquad (4.30)$$

where

$$\lambda(r) = \frac{1}{\sqrt{\pi}} \int_0^\infty d\xi\, e^{-\xi^2} \left\{ 81\left(3 + 2\xi\frac{\partial}{\partial\xi}\right)\left(8\frac{(c\tilde{c}-1)^3}{(c-\tilde{c})^6} + 2\frac{(c\tilde{c}-1)(c\tilde{c}-4)}{(c-\tilde{c})^4} - \frac{1}{(c-\tilde{c})^2}\right) \right.$$
$$\left. + 324\xi r^2 s\tilde{s}\left(36\frac{(c\tilde{c}-1)^3}{(c-\tilde{c})^8} + 6\frac{(c\tilde{c}-1)(2c\tilde{c}-5)}{(c-\tilde{c})^6} + \frac{c\tilde{c}-4}{(c-\tilde{c})^4}\right) \right\}, \qquad (4.31)$$

with $c \equiv \cosh(r\sqrt{3\xi})$, $\tilde{c} \equiv \cos(r\sqrt{3\xi})$, $s \equiv \sinh(r\sqrt{3\xi})$ and $\tilde{s} \equiv \sin(r\sqrt{3\xi})$. This function is plotted in figure 18 together with the average value $\langle \omega_1 \omega_2 \rangle_r = \lambda(r)/\sigma(r)$. At small r, the quantity between curly brackets in (4.31) behaves as $(36/35)\xi^2 r^4$, leading to $\lambda(r) \sim (9/35)r^4$ and $\langle \omega_1 \omega_2 \rangle_r \sim (3/20)r^4$. We thus recover an area of order n in the larger domain and an area of order $(3/20)nr^4 = (3/20)i^4$ in the smaller one, in agreement with the finite i result (3.34). For an arbitrary finite value of r, both ω_1 and ω_2 are finite, leading to two domains whose area is proportional to n. This indicates that exceptional points are reachable by two geodesics which are truly distinct, even in the continuum limit, as they separate macroscopic domains
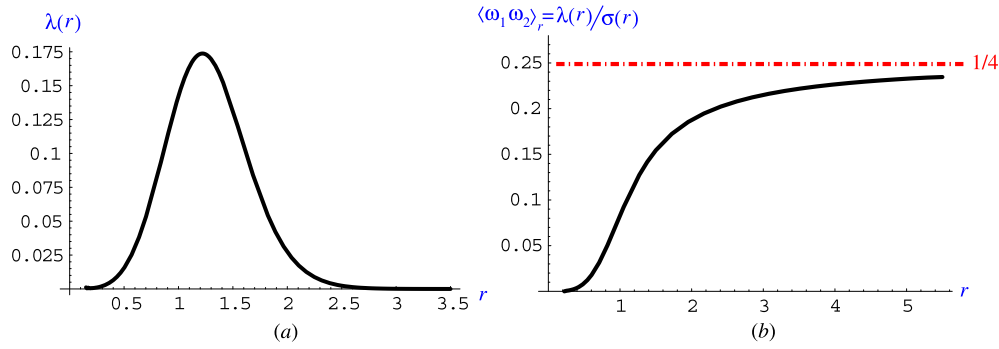
24

Figure 18. The scaling function $\lambda(r)$ of equation (4.31) and the ratio $\lambda(r)/\sigma(r)$ measuring the correlation $\langle\omega_1\omega_2\rangle_r$ for the fractions of areas ω_1 and ω_2 of the two domains delimited by two strongly avoiding confluent geodesics. The average is for geodesics leading to a given exceptional point at a distance r from the origin. For small r, $\lambda(r)/\sigma(r) \sim (3/20)r^4$, which means that the larger fraction of area is of order 1 and the smaller of order r^4. For large r, $\lambda(r)/\sigma(r) \to 1/4$, which means that both fractions tend to 1/2.

of extensive area. Finally, for large r, $\lambda(r)$ vanishes like $e^{-3(3/2)^{2/3}r^{4/3}}$ as $\sigma(r)$, with a limiting ratio

$$\frac{\lambda(r)}{\sigma(r)} \overset{r\to\infty}{\to} \frac{1}{4}. \tag{4.32}$$

Now we note that we have necessarily $\omega_1\omega_2 \leqslant 1/4$ since ω_1 and ω_2 are real positive numbers adding to 1 and we have equality only for $\omega_1 = \omega_2 = 1/2$. The large r limiting average value $\langle\omega_1\omega_2\rangle = 1/4$ therefore indicates that the exceptional points sitting at a large rescaled distance r from the origin separate the quadrangulation in two domains of equal area $n/2$. Note that such exceptional points may appear only in pointed quadrangulations with a rescaled radius larger than r, which are exponentially rare.

5. Conclusion

In this paper, we have presented a number of exact results on the statistics of geodesics in quadrangulations of large size n. At a discrete level, the number of geodesics between any two vertices at a distance i from each other grows like 3×2^i at large i. For a generic pair of vertices, any two geodesics linking these vertices stick to each other in the sense that their number of contacts is proportional to i. Moreover, they separate the quadrangulation in two very asymmetric domains, with the larger domain containing most of the area of the quadrangulation, while the smaller one has an area of order $i^3 \ll n$. This symmetry breaking extends to the case of k-tuples of geodesics, for which only one of the k domains which they form in the quadrangulation has an area of order n.

Upon factoring out the entropy factor 3×2^i, a sensible scaling limit can be reached in the regime $i = rn^{1/4}$. In this limit, the density of geodesics of rescaled length r simply coincides with the density of vertices at distance r. Similarly, for k-tuples of geodesics, we obtain the same density upon dividing by the entropy factor $k(3 \times 2^i)^k$, where the first k prefactor is an expression of the above-mentioned symmetry breaking phenomenon. A possible interpretation of these results is that there is essentially a unique geodesic path between any two points in the scaling limit and that the entropy factors simply account for a degeneracy at a microscopic level. More studies are however necessary to validate this picture. In particular, we noted that the area enclosed by two geodesics, although negligible with respect to n, still scales as $n^{3/4}$,

i.e. faster than the length $i \propto n^{1/4}$ of the geodesics. Viewing the two geodesics as forming a sequence of blobs without contact, this means that at least one of these blobs has an area larger than $n^{1/2}$. It is not clear whether the observed scaling is sufficient to guarantee that we can simply ignore the domain trapped between the geodesics in the scaling limit.

In addition to this generic behavior, we also found that, for a given origin vertex, there is a number of order $n^{1/4}$ of exceptional points that can be linked to this origin by two truly distinct geodesics with no contacts on the way. Both domains separated by the geodesics have an area proportional to n in this case. We explicited the density of these exceptional endpoints in the scaling limit as a function of the rescaled distance r but a more detailed analysis of their correlations would be desirable to understand better the geometry of this set of points.

It would be nice to extend our results to other families of maps. We expect in general that the precise value of the degeneracy factors counting discrete geodesic paths will depend on the family at hand but that all our results in the scaling limit should remain unchanged. This holds for maps in the universality class of so-called 'pure gravity'. Studying models of maps with matter degrees of freedom is another story which requires new insights.

Appendix A. Average number of contacts between two confluent geodesics

We compute here in the scaling limit $i = rn^{1/4}$ the average number of contact vertices between two weakly avoiding confluent geodesics of length i. To this end, it is convenient to introduce the generating function $Z_i^{pp}(g)$ of quadrangulations with a geodesic boundary of length i and with a *marked pinch point*. We have the relation

$$Z_i^{pp} = \sum_{j=1}^{i-1} Z_j Z_{i-j}, \tag{A.1}$$

which simply expresses that the marked pinch point, at arbitrary distance j, separates the quadrangulation with a boundary in two parts of length j and $i - j$.

To treat the case of two geodesic paths with a marked contact, we simply have to consider the generating function $2Z_i Z_i^{pp}$, which counts quadrangulations with a geodesic boundary of length $2i$, with a marked geodesic path in-between, and with a marked contact between this geodesic path and either side of the boundary. Note that if the two boundaries come into contact, the corresponding pinch point is actually counted twice. For a proper enumeration of quadrangulations with marked geodesics, we must as usual take an irreducible part. In the same way as the irreducible part $U_i^{(2)}$ of Z_i^2 counts quadrangulations with two weakly avoiding confluent geodesics, the irreducible part $U_i^{(2)pp}$ of $2Z_i Z_i^{pp}$ counts these same objects with a marked contact. It is obtained by removing configurations where the two boundaries come into contact, which translates into the relation

$$U_i^{(2)pp} = \left(2Z_i Z_i^{pp}\right) - \sum_{j=1}^{i-1} \left(U_j^{(2)} \times 2Z_{i-j} Z_{i-j}^{pp} + U_j^{(2)} \times 2Z_{i-j}^2 + U_j^{(2)pp} \times Z_{i-j}^2\right), \tag{A.2}$$

where the subtracted terms correspond to configurations where the two boundaries have a first contact at a distance j from the origin. This contact may be before the marked pinch point (first term in the sum), at the marked pinch point (second term) or after the marked pinch point (third term).

As before, the above relations transform into simple relations for the generating functions:

$$
\hat{Z}(t) \equiv \sum_{i=1}^{\infty} Z_i t^i, \qquad\qquad \hat{Z}^{(2)}(t) \equiv \sum_{i=1}^{\infty} Z_i^2 t^i, \qquad\qquad \hat{Z}^{pp}(t) \equiv \sum_{i=1}^{\infty} Z_i^{pp} t^i,
$$

$$
\hat{Z}^{(2)pp}(t) \equiv \sum_{i=1}^{\infty} 2 Z_i Z_i^{pp} t^i, \qquad \hat{U}^{(2)pp}(t) \equiv \sum_{i=1}^{\infty} U_i^{(2)pp} t^i, \qquad \hat{U}^{(2)}(t) \equiv \sum_{i=1}^{\infty} U_i^{(2)} t^i.
$$

(A.3)

Indeed, equation (A.1) translates into

$$
\hat{Z}^{pp}(t) = (\hat{Z}(t))^2
$$

(A.4)

and, using the relation $\hat{U}^{(2)}(t) = \hat{Z}^{(2)}(t)/(1 + \hat{Z}^{(2)}(t))$, equation (A.2) becomes simply

$$
\hat{U}^{(2)pp}(t) = \frac{\hat{Z}^{(2)pp}(t) - 2(\hat{Z}^{(2)}(t))^2}{(1 + \hat{Z}^{(2)}(t))^2}.
$$

(A.5)

As in section 4.2, in order to expand all the above generating functions in the scaling limit, it is convenient to treat separately their values right at $\xi = 0$, i.e. when $g = g_{\text{crit}} = 1/12$. Beyond the quantities $A_i \equiv Z_i(1/12)$, $A_i^{(2)} \equiv (A_i)^2$ and their generating functions $\hat{A}(t)$ and $\hat{A}^{(2)}(t)$ already defined in sections 3.2 and 3.3, we also introduce the notations

$$
A_i^{pp} \equiv \sum_{j=1}^{i-1} A_j A_{i-j}, \qquad \hat{A}^{pp}(t) \equiv \sum_{i-1}^{\infty} A_i^{pp} t^i = (\hat{A}(t))^2, \qquad \hat{A}^{(2)pp}(t) = \sum_{i-1}^{\infty} 2 A_i A_i^{pp} t^i.
$$

(A.6)

From equations (A.4), (4.10) and (4.11), we have the expansion

$$
\hat{Z}^{pp}\left(\frac{1}{2}\,e^{-sn^{-1/4}}\right) - \hat{A}^{pp}\left(\frac{1}{2}\,e^{-sn^{-1/4}}\right) = \frac{2n^{1/4}}{3s} \int_0^{\infty} dr\, e^{-sr} \left(\mathcal{F}(r, \xi) - \frac{2}{3r}\right) + \cdots
$$

(A.7)

from which we deduce the scaling behavior

$$
\frac{1}{2^i}\left(Z_i^{pp} - A_i^{pp}\right) = \frac{2}{3} \int_0^r dr' \left(\mathcal{F}(r', \xi) - \frac{2}{3r'}\right) + \cdots.
$$

(A.8)

This expansion, together with expansion (4.9) for $Z_i - A_i$, leads to

$$
\frac{1}{(2^i)^2}\left(2 Z_i Z_i^{pp} - 2 A_i A_i^{pp}\right) = \frac{2r}{9}\left(\mathcal{F}(r, \xi) - \frac{2}{3r}\right) + \frac{4}{9}\int_0^r dr'\left(\mathcal{F}(r', \xi) - \frac{2}{3r'}\right) + \cdots,
$$

(A.9)

where we also made use of the large i leading values $A_i/2^i \sim 1/3$ and $A_i^{pp}/2^i \sim i/9 = n^{1/4}r/9$. This yields

$$
\hat{Z}^{(2)pp}\left(\frac{1}{4}\,e^{-sn^{-1/4}}\right) - \hat{A}^{(2)pp}\left(\frac{1}{4}\,e^{-sn^{-1/4}}\right)
$$

$$
= \frac{2n^{1/4}}{9} \int_0^{\infty} dr\, e^{-sr} \left\{r\left(\mathcal{F}(r, \xi) - \frac{2}{3r}\right) + 2\int_0^r dr'\left(\mathcal{F}(r', \xi) - \frac{2}{3r'}\right)\right\} + \cdots
$$

(A.10)

while, from

$$
\frac{1}{(2^i)^2}\left(Z_i^2 - A_i^2\right) = \frac{2}{3n^{1/4}}\left(\mathcal{F}(r, \xi) - \frac{2}{3r}\right) + \cdots
$$

(A.11)

we have

$$\hat{Z}^{(2)}\left(\frac{1}{4}\,\mathrm{e}^{-sn^{-1/4}}\right) - \hat{A}^{(2)}\left(\frac{1}{4}\,\mathrm{e}^{-sn^{-1/4}}\right) = \frac{2}{3}\int_0^\infty \mathrm{d}r\,\mathrm{e}^{-sr}\left(\mathcal{F}(r,\xi)-\frac{2}{3r}\right)+\cdots. \tag{A.12}$$

Inserting expansions (A.10) and (A.12) into (A.5) and using the leading behaviors $\hat{A}^{(2)}\big(\mathrm{e}^{-sn^{-1/4}}/4\big) \sim n^{1/4}/(9s)$ and $\hat{A}^{(2)pp}\big(\mathrm{e}^{-sn^{-1/4}}/4\big) \sim 2n^{1/2}/(27s^2)$, we obtain finally

$$\hat{U}^{(2)pp}\left(\frac{1}{4}\,\mathrm{e}^{-sn^{-1/4}}\right) - \hat{W}^{(2)pp}\left(\frac{1}{4}\,\mathrm{e}^{-sn^{-1/4}}\right) = \frac{1}{n^{1/4}}\int_0^\infty \mathrm{d}r\,\mathrm{e}^{-sr}\left\{-72s\left(\mathcal{F}(r,\xi)-\frac{2}{3r}\right)\right.$$

$$\left. + 18s^2 r\left(\mathcal{F}(r,\xi)-\frac{2}{3r}\right) + 36s^2\int_0^r \mathrm{d}r'\left(\mathcal{F}(r',\xi)-\frac{2}{3r'}\right)\right\} + \cdots$$

$$= \frac{1}{n^{1/4}}\int_0^\infty \mathrm{d}r\,\mathrm{e}^{-sr}\,18r\left(\mathcal{F}''(r,\xi)-\frac{4}{3r^3}\right)+\cdots \tag{A.13}$$

upon integrations by part over r. Here we used the notation

$$\hat{W}^{(2)pp}(t) \equiv \frac{\hat{A}^{(2)pp}(t) - 2(\hat{A}^{(2)}(t))^2}{(1+\hat{A}^{(2)}(t))^2}, \tag{A.14}$$

which is the critical value of $U^{(2)pp}(t)$ at $g = 1/12$. We end up with

$$\frac{1}{(2^i)^2}\big(U_i^{(2)pp} - W_i^{(2)pp}\big) = \frac{1}{n^{1/2}}\left(18r\mathcal{F}''(r,\xi)-\frac{24}{r^2}\right)+\cdots \tag{A.15}$$

where $W_i^{(2)pp}$ is the coefficient of t^i in $\hat{W}^{(2)pp}(t)$. From the exact expression for A_i, we can easily compute $\hat{W}^{(2)pp}(t)$ exactly. In particular, we have the small η expansion:

$$\hat{W}^{(2)pp}\big(\tfrac{1}{4}(1-\eta)\big) = 4 + (12 - 8\pi^2 + 24\log(\eta))\eta + \mathcal{O}(\eta^2). \tag{A.16}$$

From the singularity at $\eta = 0$, we deduce that $W_i^{(2)pp}/(2^i)^2 \sim 24/i^2 = 24/(n^{1/2}r^2)$ in the scaling regime, and therefore

$$\frac{1}{(2^i)^2}U_i^{(2)pp} = \frac{18}{n^{1/2}}r\mathcal{F}''(r,\xi)+\cdots. \tag{A.17}$$

Upon integration over ξ, this gives finally

$$\left.\frac{U_i^{(2)pp}}{(2^i)^2}\right|_{g^n} \overset{n\to\infty}{\sim} \frac{12^n}{\pi n^{3/2}}18r\int_{-\infty}^{+\infty}\mathrm{d}\xi\,\xi\,\mathrm{e}^{-\xi^2}\mathcal{F}''(r,\xi). \tag{A.18}$$

Dividing this result by

$$\left.\frac{U_i^{(2)}}{(2^i)^2}\right|_{g^n} \overset{n\to\infty}{\sim} \frac{12^n}{\pi n^{7/4}}54\int_{-\infty}^{+\infty}\mathrm{d}\xi\,\xi\,\mathrm{e}^{-\xi^2}\mathcal{F}''(r,\xi) \tag{A.19}$$

yields the average number of contacts

$$\langle c\rangle_r = n^{1/4}\frac{r}{3}. \tag{A.20}$$

For small r, this gives the finite i result $\langle c\rangle_i = \frac{i}{3}$ of equation (3.26). The linear dependence of the average number of contacts extends in practice to the whole range of r in the scaling limit.

28

Appendix B. Correction to the area correlation for two weakly avoiding geodesics

The scaling result (4.28), i.e. $\langle \omega_1 \omega_2 \rangle_r = 0$ for two weakly avoiding confluent geodesics holds in the scaling limit $n \to \infty$. We can easily get the first correction to scaling by computing the $1/n$ term in equation (4.25) giving $U_i^{(2)}(g; \lambda_1, \lambda_2)/(2^i)^2$. In practice, as we eventually apply the operator $1/(4\mu_1\mu_2)\partial^2/\partial\mu_1\partial\mu_2$, we need only the corresponding cross-term depending on both μ_1 and μ_2. This term reads

$$\frac{81}{n}\left\{\frac{\partial^2}{\partial r^2}\left(\mathcal{F}(r,\mu_1)\mathcal{F}(r,\mu_2)-\frac{4}{9r^2}\right)\right.$$
$$\left.-2\frac{\partial^3}{\partial r^3}\left(\int_0^r \mathrm{d}r'\left(\mathcal{F}(r',\mu_1)-\frac{2}{3r'}\right)\left(\mathcal{F}(r-r',\mu_2)-\frac{2}{3(r-r')}\right)\right)\right\}. \quad (B.1)$$

This leads immediately to the correction

$$\langle \omega_1 \omega_2 \rangle_r = \frac{9}{n^{1/4}\rho(r)}\frac{1}{\mathrm{i}\sqrt{\pi}}\int_{-\infty}^{+\infty}\mathrm{d}\xi\,\xi\,\mathrm{e}^{-\xi^2}\left\{\frac{\partial^2}{\partial r^2}\left(\frac{1}{2\xi}\frac{\partial\mathcal{F}}{\partial\xi}(r,\xi)\right)^2\right.$$
$$\left.-2\frac{\partial^3}{\partial r^3}\left(\int_0^r\mathrm{d}r'\frac{1}{2\xi}\frac{\partial\mathcal{F}}{\partial\xi}(r',\xi)\frac{1}{2\xi}\frac{\partial\mathcal{F}}{\partial\xi}(r-r',\xi)\right)\right\}. \quad (B.2)$$

In particular, at small r, we have the expansion

$$\frac{1}{2\xi}\frac{\partial\mathcal{F}}{\partial\xi}(r,\xi) = \frac{r^3}{30}+\mathrm{i}\xi\frac{r^5}{140}+\cdots \quad (B.3)$$

so that the $\{\cdot\}$ term in the integrand of equation (B.2) behaves as

$$\frac{3}{100}r^4+\mathrm{i}\xi\frac{9}{350}r^6+\cdots. \quad (B.4)$$

Upon integration over ξ, only the second term survives so that the integral behaves as $\mathrm{i}\sqrt{\pi}\times 9r^6/700$. From the small r behavior $\rho(r) \sim 3r^3/7$, we deduce

$$\langle \omega_1 \omega_2 \rangle_r \overset{r\to 0}{\sim} \frac{1}{n^{1/4}}\frac{27}{100}r^3, \quad (B.5)$$

which is nothing but the announced result (3.28).

References

[1] Kazakov V 1985 Bilocal regularization of models of random surfaces *Phys. Lett.* B **150** 282–4
    David F 1985 Planar diagrams, two-dimensional lattice gravity and surface models *Nucl. Phys.* B **257** 45–58
    Ambjorn J, Durhuus B and Fröhlich J 1985 Diseases of triangulated random surface models and possible cures
        Nucl. Phys. B **257** 433–49
    Kazakov V, Kostov I and Migdal A 1985 Critical properties of randomly triangulated planar random surfaces
        Phys. Lett. B **157** 295–300
[2] Tutte W 1962 A Census of planar triangulations *Can. J. Math.* **14** 21–38
    Tutte W 1962 A Census of Hamiltonian polygons *Can. J. Math.* **14** 402–17
    Tutte W 1962 A Census of slicings *Can. J. Math.* **14** 708–22
    Tutte W 1963 A Census of planar maps *Can. J. Math.* **15** 249–71
[3] Brézin E, Itzykson C, Parisi G and Zuber J-B 1978 Planar diagrams *Commun. Math. Phys.* **59** 35–51
[4] Di Francesco P, Ginsparg P and Zinn-Justin J 1995 2D gravity and random matrices *Phys. Rep.* **254** 1–131
[5] Ambjørn J and Watabiki Y 1995 Scaling in quantum gravity *Nucl. Phys.* B **445** 129–44
[6] Ambjørn J, Jurkiewicz J and Watabiki Y 1995 On the fractal structure of two-dimensional quantum gravity
    Nucl. Phys. B **454** 313–42
[7] Marcus M and Schaeffer G 2001 Une bijection simple pour les cartes orientables (available at http://www.lix.polytechnique.fr/Labo/Gilles.Schaeffer/Biblio/)

[8] Chassaing P and Schaeffer G 2004 Random planar lattices and integrated superBrownian excursion *Probab. Theory Relat. Fields* **128** 161–212 (*Preprint* math.CO/0205226)

[9] Bouttier J, Di Francesco P and Guitter E 2004 Planar maps as labeled mobiles *Elec. J. Comb.* **11** R69 (*Preprint* math.CO/0405099)

[10] Bouttier J, Di Francesco P and Guitter E 2007 Blocked edges on Eulerian maps and mobiles: application to spanning trees, hard particles and the Ising model *J. Phys. A: Math. Theor.* **40** 7411–40 (*Preprint* math.CO/0702097)

[11] Bouttier J, Di Francesco P and Guitter E 2003 Geodesic distance in planar graphs *Nucl. Phys.* B **663** 535–67 (*Preprint* cond-mat/0303272)

[12] Marckert J F and Mokkadem A 2006 Limit of normalized quadrangulations: the Brownian map *Ann. Probab.* **34** 2144–2202 (*Preprint* math.PR/0403398)

[13] Le Gall J-F 2006 The topological structure of scaling limits of large planar maps *Preprint* math.PR/0607567

[14] Le Gall J-F and Paulin F 2006 Scaling limits of bipartite planar maps are homeomorphic to the 2-sphere *Preprint* math.PR/0612315

[15] Cori R and Vauquelin B 1981 Planar maps are well labeled trees *Can. J. Math.* **33** 1023–42